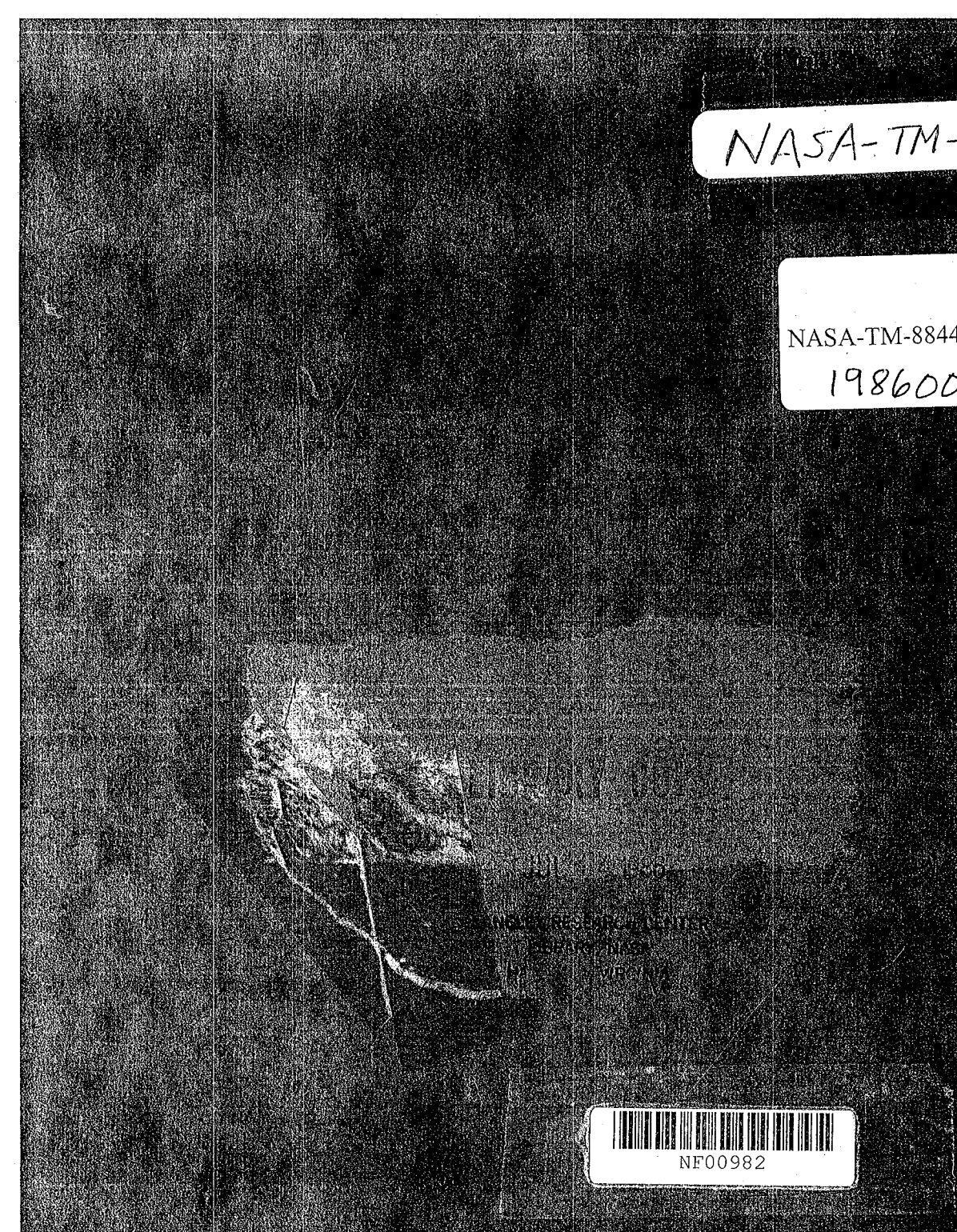

NASA TECHNICAL MEMORANDUM NASA TM-88444

INITIAL ADAPTATION TESTING OF THE BIDIMENSIONALLY SELF-ADAPTING WALL OF THE FRENCH T2 WIND TUNNEL, AROUND A THREE-DIMENSIONAL OBJECT

J.P. Archambaud, J.B. Dor, A. Mignosi and L. Lamarche

Translation of: "Premiers essais d'adaptation des parois auto-adaptables bidimensionnelles de la soufflerie T2 autour d'obstacles tridimensionnels." Rapport technique OA 33/3075 (DERAT 11/5015 DN), O.N.E.R.A., Centre d' Etudes et de Recherches de Toulouse, France, September 1985, pp. 1-49.

NATIONAL AERONAUTICS AND SPACE ADMINISTRATION
WASHINGTON D.C. 20546 JUNE 1986

STANDARD TITLE PAGE

1. Report No.	2. Government Accession No.	3. Recipient's Catalog No.
NASA TM-88444		

4. Title and Subtitle	5. Report Date
INITIAL ADAPTATION TESTING OF THE BIDIMENSIONALLY SELF-ADAPTING WALL OF THE FRENCH T2 WIND TUNNEL, AROUND A THREE-DIMENSIONAL OBJECT	JUNE 1986
	6. Performing Organization Code

7. Author(s)	8. Performing Organization Report No.
J.P. Archambaud, J.B. Dor, A. Mignosi and L. Lamarche	10. Work Unit No.

9. Performing Organization Name and Address	11. Contract or Grant No.
SCITRAN Box 5456 Santa Barbara, CA 93108	NASw- 4004
	13. Type of Report and Period Covered Translation
12. Sponsoring Agency Name and Address National Aeronautics and Space Administration Washington, D.C. 20546	14. Sponsoring Agency Code

15. Supplementary Notes

Translation of:"Premiers essais d'adaptation des parois auto-adaptables bidimensionnelles de la soufflerie T2 autour d'obstacles tridimensionnels." Rapport technique OA 33/3075 (DERAT 11/5015 DN), O.N.E.R.A., Centre d' Etudes et de Recherches de Toulouse, France, September 1985, pp. 1-49.

16. Abstract

The test series were carried out at ONERA/CERT at the T2 wind tunnel in September 1984. The objective of this series was to minimize wall interference through a bidimensional adaptation around the models, inducing tridimensional flows. For this, we used three different models by measuring either the pressures or the forces and moment of pitch (balance). The adaptation was derived from a correction computation in the compressible axisymmetric tridimensional.

17. Key Words (Selected by Author(s))	18. Distribution Statement
	Unclassified and Unlimited

19. Security Classif. (of this report)	20. Security Classif. (of this page)	21. No. of Pages	22. Price
Unclassified	Unclassified	52	

TM88444 TOULOUSE ENGINEERING AND RESEARCH CENTER

2 Avenue Edouard Belin--31055 TOULOUSE CEDEX

DEPARTMENT OF ENGINEERING AND RESEARCH

IN AERODYNAMICS

Engineering Report OA 33/3075 AND (DERAT 11/5015 DN)- Sept 1985

First tests of adaptation of bidimensional adaptive walls in the T2 wind tunnel around tridimensional obstacles.

by J.P. ARCHAMBAUD /s/ J.B. DOR /s/ A. MIGNOSI /s/ L. LAMARCHE /s/

D.E.R.A.T. Director

R.MICHEL
/s/

/3/ *

AUTHOR'S ABSTRACT

These tests carried out in September 1984 constitute the first approach to adaptation of tridimensional flow. The deformation of the walls remains bidimensional (as in the preceding test series). But the computation of these deformations is the result of a method of estimation of wall interferences in the tridimensional.

Three models have been tested:

- C 5 rotation body
- model of the F 4 transport aircraft
- model of a delta wing canard aircraft

The adaptation around the C 5 body had the objective of comparison with the results of a true tridimensional adaptation (TU-Berlin) and tests in a large wind tunnel (NASA Ames).

*Numbers in margin indicate foreign pagination.

NOTATIONS

B	test section airflow width
C	model length
C_L	coefficient of length
C_M	coefficient of pitch
C_D	coefficient of drag
H	height of test section airflow
M_o	test infinite Mach number
PT	total pressure
RC	Reynolds number of the flow (linked to C)
TT	total temperature
x, y, z	Cartesian coordinates orthonormalized reference

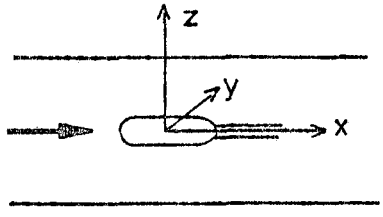

2D	abbreviation for bidimensional
3D	abbreviation for tridimensional
α	angle of incidence announced before the test
α_c	corrected angle of incidence (by balance measurements or photographic measurements)
v.g.	vertical generatrix } NASA Ames test
h.g.	horizontal generatrix }

1. INTRODUCTION

The test series presented below were carried out at ONERA/CERT at the T2 wind tunnel in September 1984. It was carried out in close collaboration with Prof. U. GANZER and his associates MM. Y. IGETA and J.ZIEMANN at the University of Berlin.

The objective of this series was to minimize wall interference through a bidimensional adaptation around the models, inducing tridimensional flows.

For this, we used three different models by measuring either the pressures or the forces and moment of pitch (balance). The adaptation was derived from a correction computation in the compressible axisymmetric tridimensional.

2. GENERALIZATIONS

2.1. T2 Wind Tunnel

The T2 wind tunnel is a closed loop installation with induction operation with 1 to 2 minute gusts (PL.1) /REF. 1 and 2/.

Its test section airflow (H = 370mm, B = 390mm, at the inlet) is equipped with flexible upper and lower walls (PL.1), each activated by 16 jacks. Each deformable wall is equipped with 58 central pressure ports (Ø = 0.4mm) and with some lateral ports. In addition, the left vertical wall also has pressure ports arranged in three horizontal and three vertical lines. Only the central ports will be used during the adaptation; the others make possible verification of satisfactory coherence of the velocity field only in some cases.

2.2. Models--balance--sting model support

The three models used are;

- axisymmetric C5 body c = 166.25mm
- F4 aircraft C = 119.9mm
- delta wing canard C = 145mm

The C5 body is an aximetrique model formed of an assembly of geometrically simple elements (PL. 2 and 3). The body has been tested in numerous installations which makes possible the comparison of interesting results; to wit: 3D adaptive walls TU Berlin--16 ft AEDC--11 ft NASA Ames, 6 ft S2 Modane ONERA.

The model called the F4 is one of an Airbus type aircraft and has supercritical wings (PL.4). The third model represents /7/ a supersonic delta winged aircraft equipped with two small canard-type ailerons at the front.

A balance of very small overall dimension (Ø = 8mm) furnishes the axial and normal loads and the pitch moment working on the model. Knowledge of the loads and of the pitch moment also makes possible definition of the actual angle of incidence. This balance is adaptable to two aircraft models. The electrical voltages associated with the different components are obtained in real time and recorded by the acquisition system.

The various models are held by a sting support (see PL.2) the diameter of which creats a tiny perturbation on a length of about a chord. Further downstream, this sting is connected to a rather voluminous gimbal joint centered approximately 2 chords behind the profile, towards the downstream end of the adaptive walls; the overall bulk of this obstacle will therefore be compensated by the adaptation of the airflow section, thus avoiding a very strong corresponding perturbation and its upstream extension very far towards the model. The part at the rear of this gimbal is fixed to a rod which lies across the second throat and pivots around an axis of rotation 1.5mm downstream of the model.

2.3 Adaptation of the upper and lower wall

The physical displacement of the adaptive upper and lower walls is bidimensional (REF. 3/. But the deformations computed by the program for adaptation /REF. 4/ take into account the tridimensional character of the flow. With this end in view, the model is designed for the distributions of 3D sources and of horseshoe vortices (of infinitely small dimensions) located on the airflow axis. The pressure measurements on the upper and lower walls give access to the intensities of these singularities. The interference of the walls is thus estimated by means of external imaging at the level of the airflow axis. It is next cancelled out by an appropriate new formation to the walls. Actually, two linear operators, uniquely dependent on the test section geometry, make it possible to go directly from parietal pressure measurements to the adaptive forms. The compressibility is taken into account by

the presence of the factor $\beta = \sqrt{1 - M_o^2}$. The method thus described consists of a single iteration.

The releasing thus created around each of the three models is not very important due to the small overall dimension of these obstacles in the T2 test section. On the other hand the sting model support with its relatively voluminous gimbal (PL.2) causes a strong divergence of the adaptive walls which is frequently insufficient (lower wall in extreme position--Plate 7). However, in all the cases presented the perturbations caused by the model and the sting seem well decoupled in the wall area: either because these perturbations are initially weak and little extended between non-adapted walls ($M_o < 0.7$), or because the adaptation diminishes and localizes the sting perturbation in the more rigorous configurations.

In the following part of this report we will term "non-adapted walls" a simple divergent configuration designed to compensate the convergence due to the boundary layers developing on the four walls of the test section airflow (vertical walls considered as plane plates /REF. 3/). The expression "adapted walls" will designate the wall forms produced by the adaptation computation in a stage described below.

2.4 Test configurations /8/

The test configurations are given in Tables 1, 2 and 3, and are visualized in the following synoptic diagram:

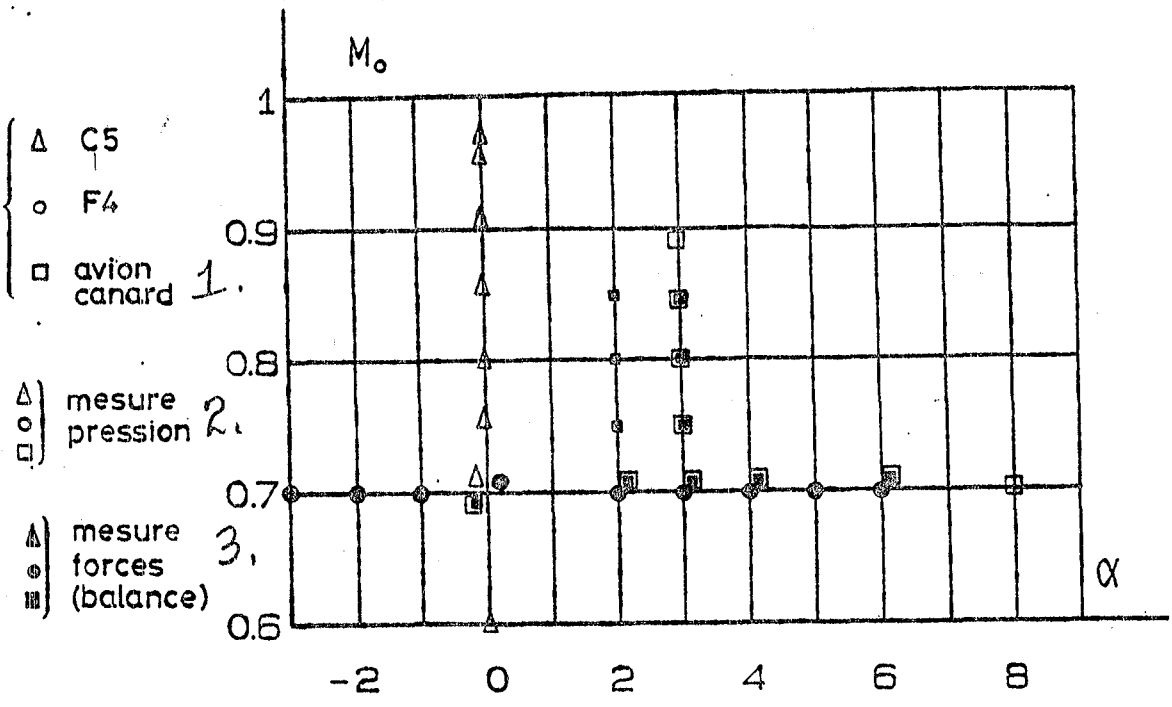

1. canard aircraft
2. pressure measurement
3. measurement of forces (balance)

When the balance is not employed, the angle of incidence α examined in the plots is that measured before the run. Indeed the rigid assembly does not prevent a slight variation in this angle during the run . We have been supplied by Mr GANZER with this incidence correction measured by means of photos; it is plotted in Figure 32 and can serve to correct the corresponding plots in this type test. On the other hand, when the balance is used, this angle correction, systematically computed, is reflected in all the corresponding results in this type test. Verification with a cathetometer during run also makes it possible to check out the satisfactory precision of this correction on several tests carried out with the F4 aircraft model.

The test Mach number M_o is determined from the distributions of Mach number measured on the upper and lower walls. It involves an average in space. Local deviations with respect to M_o are slight for $M_o \leq 0.85$; these deviations then overlap D_o for $M_o > 0.85$; (see PL. 5 and 6).

For each test configuration (except for the C5 body, $M_o = 0.70$, $\alpha = 0^o$) two runs are necessary. The first is carried out

between non-adaptive walls, and makes use of the computational base for the adaptive forms which will be used in the second run ; /9/ this second test allows pressure and aerodynamic parameter measurements while minimizing the interaction of the walls.

All the tests were carried out at ambient temperatures with a pressure generatrix between 1.6 b and 2.2 bar.

3 - C 5 BODY

The model (PL.3) provided by TU Berlin for the more reduced test sections, presents a slight overall dimension in the T2 wind tunnel ($S_{\text{max cross section}}/S_{\text{test section}} \cong 3.1^{o}/oo$). It has been tested at zero incidence, and the measurements carried out are pressure measurments using 20 pressure ports.

The following table gives some accuracies in the cases covered:

M_o	0.6	0.7	0.843	0.915	0.93	0.95	0.97
T2 upper and lower wall	adapted	non-adapted	adapted	adapted	adapted	adapted	adapted
Comparison with		TU Berlin NASA Ames	TU Berlin NASA Ames			NASA Ames	NASA Ames

3.1. Walls

In plates 5 and 6 one confirms the faint signature of the model on the flexible walls, as long as $M_o < 0.85$. Above this, this influence is likely to be more and more significant.

In all the cases accomodated one notes the inadequacy of the unblocking of the test section foreseen by the correction calculation for the site of the gimbal. This phenomenon is strongly accentuated when M_o increases above 0.85. However, all the tests show that this perturbation does not increase enough upstream to interfere with those which are ascribable to the model.

The lack of parallelism of the walls appears in the form of a modulation around the M_o value upstream of the model. The amplitude of this modulation grows with M_o. We are dealing here with slight bulging of the wall between the jacks which seem to alternately succeed one another in the direction of the test section and then toward the exterior. They are the results of a complex combination

of several parameters: the pressure differences between the interior of the test section and the exterior container, upstream tail-in, flexure of the sheet metal, and the relative position of "fixed" points (rotation possible) at the site of the jacks.

Plate 7 shows the wall shapes. The central shape, simply divergent, has been called the non-adapted shape. (see sec. 2.3.). The other evolutions proceed from the adaptation computation. One sees a trend at the opening even before the first jacks, upstream of the test section. Unblocking is very weak at the site of the model. On the other hand, downstream the walls are strongly divergent but insufficiently, as mentioned above. A certain dissymmetry between the upper and lower shapes can be determined at the sites of the two upstream rear jacks; indeed on the lower wall the rearmost jack is at the extreme position in all cases and also the next to last jack for $M_o > 0.95$.

Note : Plates 8 and 9 present the distributions of pressure measured to the right of the model on three walls: upper, lower and the left side.

In Plate 8, around the axisymmetric C5 body, the various curves seem to be in good agreement except around x = +100mm (towards the base of the model) where a minimum Mach number is recorded more pronounced on the lower wall.

On Plate 9 (canard aircraft- $\alpha = 8^{o}$--non-adapted walls) there can clearly be perceived the continued diminution of the pressure perturbation when it passes through the demi-perimeter of the test section airflow by coming away from the upper wall. This evolution is coherent with the test configuration.Moreover, the symmetry with respect to the median vertical plane is verified correctly by the favorable cross-checking of the lines of pressure ports situated on the edges of the flexible walls. However, the pressure distributions on the downstream portion of the lower wall x = 0 presents the same defect as in Plate 8, i.e. a trough preceded here by an equally abnormal spike; these anomalies recurred in a certain number of tests and seem attributable to an imperfection in the sheet-metal.

It is interesting to note that these pressure distributions recorded on the plane and rigid lateral wall flow much better than those measured on the flexible walls.

3.2. Model

Oil visualization carried out (PL.3) on the model at $M_o = 0.6$ shows that the laminar flow at the stagnation point (dark zone) transitions before the central bulge (distinct cones of untimely release).

Plates 10 and 11 show the distributions of Mach number on the C 5 body in the different cases studied, (except for $0.7 < M_o < 0.84$).

For $M_o < 0.85$ (PL.10), the general shape of the run is preserved, whereas the maximum value around x/c = 50% perceptibly increases with M_o. Plate 8 ($M_o > 0.84$) indicates a strong widening of the median supercritical zone as M_o increases, on account of the shock recoil; in parallel, at the base of this shock, a separation causes an overloading of the velocity minimum between 60% and 80% of chord.

Plates 12 and 13 make possible a comparison of the results /11/ obtained with the same model at Berlin (TU Berlin- 2D and 3D adaptation, /REF. 5/) and at ONERA/CERT (T2, 2D adaptation based on a 3D correction). On the whole the cross-checks are good; at $M_o = 0.7$ (PL.12) the results of the 2D adaptations are very coherent, whereas the 3D adaptation (TU Berlin) appears to unblock the more slightly in certain zones. Around $M_o = 0.84$ (PL. 13) the Mach number distribution produced by TU Berlin ($M_o = 0.84$) is well inserted between the two readings taken at T2 ($M_o = 0.832$ and 0.843.

A comparison is also made between the results at NASA Ames /REF.6/ on plates 14,15,16 and 17 respectively for $M_o = 0.7$, 0.84, 0.95, and 0.97. The model used at Ames involves two rows of ports drilled on two generatrices located in the perpendicular plane. It is approximately 6.4 times longer and the transition is released around about the stagnation point by ballottines. The results are in good agreement; at $M_o = .097$, downstream of the central bulge the Reynolds effect seems to diminish the intensity of the shock/boundary layer interaction in the case of NASA Ames compared to T2.

3.3. Comparison of experiment and computation

Two cross-check tests of measurements, carried out at T2 by

computations were done, one on the model, the other on the walls.

The model has been schematicized by an aggregate of panels of uniformly loaded sources; the velocity is calculated for compressibility using the Goethert's rule of similitude, valid for subsonic circulating flow. A generatrix comprises 90 panels and a transverse section 32. For the infinite Mach numbers considered (M_o = -0.6- 0.7- 0.84), good experiment/computation agreement is established for the whole of the model (PL.18), mainly at the extreme segments. The central spike is nicely reproduced by the computation for M_o = 0.6 and 0.7; however a small deviation appears for M_o = 0.84 (sonic peak) and one could surmise a viscosity effect and an imprecision in the similitude rule.

The model mount assembly (sting, gimbal, rod) has been schematicized by a series of contiguous segments of linealized doublets (constant intensity on each segment). The compressible computation was also done to include Goethert's law. The images of the doublet segments in relationship to four sides of the test section schematicize the wall interference. Plate 19 shows the distributions measured and calculated for the Mach number on the upper and lower walls in two non-adaptive cases (M_o = 0.7 and 0.84); one can confirm that this schematization predicts quite well the perturbations of the sting and its gimbal.

4- F4 AIRCRAFT

The F 4 aircraft model (PL.3) presents a very small overall dimension in the test section airflow of the T2 wind tunnel ($S/SV \equiv 2.5^{\circ}/_{oo}$) and all the tests were carried out between non-adaptive walls. Plate 20 shows the faint signature of the model /12/ on the upper and lower walls in one of the cases studied which was the configuration with the greater lift.

For this model we carried out a sweep in incidence at M_o = 0.7. The aerodynamic coefficients C_L, C_D, C_M are presented in Plate 21.

5- CANARD AIRCRAFT

5.1 Tests with balance

These tests comprised an incidence sweep ($0 < \alpha < 0.844$) at M_o = 0.70 and two sweeps in Mach number ($0.7 < M_o < 0.844$) at $\alpha = 2^{\circ}$ and 3° (selected).

Figure 22 shows the evolution of the lift coefficient C_L

as a function of the incidence angle α at $M_o = 0.7$. There is established a noticeable diminution of C_L caused by the adaptation of the flexible walls, a deviation growing with α.

Plate 23 regroups the curves C_D (C_L) and C_M (C_L) at $M_o = 0.7$

Plate 24 illustrates the increase in slope $\frac{dC_L}{d}$ as M_o grows.

On Plate 25 are plotted the values of C_L as a function of M_o for the initial incidences of $\alpha = 2^o$ and 3^o. The incidence correction given by the balance increases with M_o (see table). Reduced to a fixed incidence (incidence corrected at $M_o = 0.7$), the evolutions of C_L are quasi-rectilinear and very slightly increasing.

5.2. Tests with pressure measurements

The pressure ports number 10, of which 2 are located under the cockpit. The 8 others form a line on the side of the fuselage, above the plane of the wings.

This series of tests comprised a sweep in incidence $0 < \alpha < 8^o$ at $M_o = 0.7$ as well as a sweep in Mach $0.7 < M_o < 0.876$ at $\alpha = 3^o$.

In Plate 26 showing the distributions of Mach number on the deformable walls, one clearly sees the growing influence of the model on the upper wall when the incidence grows. The signature on the wall is never significant. We note that the incidence setting is made by rotation at the site of the gimbal, and therefore the aircraft is located above the axis of the airflow for $\alpha > 0$.

One can note on the upper wall that the bulged shape of the distribution of Mach number before adaptation dips in the middle when this adaptation takes place. We also stress the perturbation constant due to the gimbal but its interaction is more and more marked with that of the model in the non-adaptive case.

On the model (PL.27), the velocities everywhere increase /13/ with incidence, but in a more distinct manner between X/C = 50% and 75% at the wide part of the wings, the elements with the most lift.

Up to $\alpha = 6^o$, the velocity curves on the model between non-

adaptive and adaptive walls do not differ from each other. On the other hand, for $\alpha = 8^{\circ}$ (PL.28) the non-adaptive test presents an overspeed of the system on the order of $\Delta M = 0.01$ in comparison with the adapted case. It seems, from the velocity on the walls (PL.25), that the non-adaptive case corresponds roughly to a real infinite Mach number (linked to the proximity of the model) slightly more elevated; this would explain the general displacement of Mach number on the model; the effect of the incidence of non-adaption would be of a lower order.

At a fixed incidence ($\alpha = 3^{\circ}$), between non-adaptive walls, one notices (PL.29) the phenomenon observed earlier of increase and of the interaction of the perturbations of the model and the sting/gimbal assembly when M_o increases. For high values of M_o, there results a longitudinal velocity gradient. The adaptation of the walls creates unblocking of the test section in its downstream section which has a higher level of velocity.

The longitudinal gradient has also disappeared and the perturbations due to the profile and to the gimbal seem separated. Plate 31 shows a regular staging of the Mach number distributions on the profile, with a strong increase in level next to the canard wings at the front (passage to supersonic) and on the cockpit.

CONCLUSION

This series of tests is the first step towards a minimizing of the wall interferences in the tridimensional. The bidimensional adaptation of the upper and lower walls alone constitutes a priori the most rough approximation of the process; this shortcoming is, however, reduced by the fact that the profiles studied are of small overall dimensions. On the other hand, the method is grounded in a tridimensional computation and a cancellation of the wall interference on the test section airflow axis; this method, applied to a "bidimensional" test section similar to that used at T2, leads to a small residual interference according to these authors /REF.4/.

REFERENCES

/1/ MICHEL R., QUEMARD C., MIGNOSI A. The induction driven tunnel T2 of ONERA/CERT : flow qualities, testing techniques and examples of results. -Journal of Aircraft, VOL. 16. No.3 (1979)

/2/ GOBERT J.L., MIGNOSI A. Studies on the cryogenic induction driven wind tunnel T2. -ETW Cryogenic Technology Review Meeting NLR Amsterdam (1982).

/3/ CHEVALLIER J.P., MIGNOSI A., ARCHAMBAUD J.P., SERAUDI A. Adaptive walls at the T2 wind tunnel: principle, construction and some examples of bidimensional results. -La Recherche Aerospatial No. 1983-4

/4/ LAMARCHE L., WEDEMEYER E. Minimization of wall interference for three-dimensional models with two-dimensional wall adaptation. -V.K.I. Technical Note 149 (March 1984).

/5/ GANZER U., IGETA Y., ZIEMANN J. Design and operation of TU Berlin wind tunnel with adaptive walls -ICAS Paper 84-2.1.1., Sept. 1984.

/6/ VAUCHERET X., BAZIN M., ARMAND C. Comparison of bi- and tridimensional transsonic tests carried out in various wind tunnels. -AGARD CP No. 187 (1975)

1.

Corps C5 (pression)

2. ESSAI	3. ADAPTE NON AD	ALPH	M0	PT (B)	TT OK	RC E+06
AD15	NA	0.00	.697	1.601	298.	3.3
AD16	NA	0.00	.751	1.686	297.	3.7
AD17	NA	0.00	.812	1.709	298.	4.0
AD18	NA	0.00	.830	1.797	297.	4.1
AD19	NA	0.00	.835	1.864	297.	4.3
AD20	NA	0.00	.842	1.896	297.	4.4
AD22	A	0.00	.832	1.877	298.	4.3
AD23	A	0.00	.843	1.863	297.	4.3
AD24	A	0.00	.915	1.981	298.	4.7
AD25	A	0.00	.930	1.954	298.	4.7
AD26	A	0.00	.950	2.021	297.	4.9
AD28	A	0.00	.970	2.009	298.	4.9
AD29	NA	0.00	.623	1.579	296.	3.1
AD30	NA	0.00	.604	1.565	296.	3.0
AD31	A	0.00	.604	1.564	296.	3.0

4.

Avion F4 (balance)

2. ESSAI	3. ADAPTE NON AD	ALPH	ALPHC	M0	PT (B)	TT OK	RC E+06	CD	CL	CM
AD109	NA	-1.00	-.65	.699	1.615	296.	2.4	.0272	.299	-.068
AD110	NA	-2.00	-1.78	.699	1.610	295.	2.4	.0184	.212	-.091
AD111	NA	-3.00	-2.95	.698	1.593	297.	2.4	.0198	.071	-.087
AD112	NA	2.00	2.62	.699	1.601	297.	2.4	.0482	.486	.007
AD113	NA	3.00	3.69	.699	1.609	296.	2.4	.0686	.529	.024
AD114	NA	4.00	4.71	.699	1.603	297.	2.4	.0905	.547	.020
AD115	NA	5.00	5.75	.698	1.606	297.	2.4	.1092	.568	.028
AD116	NA	6.00	6.77	.698	1.594	297.	2.4	.1317	.580	.039
AD117	NA	0.00	.47	.699	1.610	297.	2.4	.0288	.387	-.044
AD118	NA	0.00	.69	.699	2.209	295.	3.3	.0251	.413	-.048

1. C5 body (pressure)
2. test
3. adaptive/non-adaptive
4. F4 aircraft

1.

2 3. Avion canard (balance)

/16/

ESSAI	ADAPTE NON AD	ALPH	ALPHC	M0	PT (B)	TT OK	RC E+06	CD	CL	CM
AD201	NA	0.00	.12	.696	1.611	298.	2.9	.0181	-.049	.029
AD202	A	0.00	.12	.700	1.605	297.	2.9	.0180	-.049	.029
AD203	NA	2.00	2.54	.702	1.615	297.	3.0	.0188	.083	.031
AD204	NA	4.00	4.98	.697	1.599	297.	2.9	.0277	.225	.033
AD206	A	4.00	4.97	.700	1.607	297.	2.9	.0276	.220	.033
AD207	NA	6.00	7.43	.696	1.606	297.	2.9	.0508	.362	.037
AD208	A	6.00	7.41	.698	1.605	297.	2.9	.0474	.352	.037
AD209	NA	3.00	3.73	.698	1.608	297.	2.9	.0217	.142	.032
AD210	A	3.00	3.76	.700	1.607	297.	2.9	.0216	.151	.033
AD211	NA	3.00	3.95	.751	1.695	296.	3.2	.0228	.171	.033
AD212	A	3.00	3.90	.755	1.630	297.	3.1	.0222	.163	.033
AD213	NA	3.00	4.02	.792	1.653	297.	3.2	.0232	.180	.033
AD214	A	3.00	4.01	.797	1.654	297.	3.3	.0226	.174	.033
AD215	NA	3.00	4.07	.798	1.687	297.	3.3	.0233	.184	.033
AD216	NA	3.00	4.09	.809	1.679	296.	3.3	.0238	.186	.032
AD217	NA	3.00	4.19	.825	1.747	297.	3.5	.0241	.195	.032
AD218	A	3.00	4.23	.844	1.759	297.	3.6	.0230	.193	.033
AD219	NA	3.00	4.18	.816	1.759	297.	3.5	.0225	.194	.032
AD220	A	3.00	4.18	.827	1.763	298.	3.5	.0229	.187	.033
AD221	A	3.00	4.23	.842	1.763	299.	3.5	.0229	.192	.033
AD222	NA	3.00	4.35	.839	1.869	298.	3.8	.0243	.207	.032
AD223	NA	2.00	2.56	.700	1.698	296.	3.1	.0176	.080	.031
AD224	A	2.00	2.55	.701	1.695	297.	3.1	.0169	.078	.031
AD225	NA	2.00	2.64	.751	1.716	296.	3.3	.0185	.086	.031
AD226	A	2.00	2.65	.755	1.719	295.	3.3	.0181	.084	.031
AD227	NA	2.00	2.78	.805	1.746	296.	3.5	.0185	.097	.034
AD228	A	2.00	2.77	.810	1.748	295.	3.5	.0184	.093	.033
AD229	NA	2.00	2.82	.824	1.753	296.	3.5	.0189	.100	.033
AD230	A	2.00	2.84	.845	1.757	296.	3.6	.0186	.098	.034
AD231	NA	2.00	2.95	.852	1.861	295.	3.8	.0194	.110	.034

4.

2 Avion canard (pression) 3

ESSAI	ADAPTE NON AD	ALPH	M0	PT (B)	TT OK	RC E+06
AD250	NA	0.00	.698	1.693	297.	3.1
AD251	A	0.00	.701	1.698	298.	3.1
AD252	NA	2.00	.696	1.698	297.	3.1
AD253	A	2.00	.699	1.694	297.	3.1
AD254	NA	4.00	.697	1.688	296.	3.1
AD255	A	4.00	.700	1.700	295.	3.1
AD256	NA	6.00	.696	1.700	296.	3.1
AD257	A	6.00	.698	1.703	297.	3.1
AD258	NA	8.00	.696	1.696	297.	3.1
AD259	A	8.00	.695	1.698	297.	3.1
AD260	NA	3.00	.698	1.695	297.	3.1
AD261	A	3.00	.700	1.694	295.	3.1
AD262	NA	3.00	.751	1.726	296.	3.3
AD263	A	3.00	.757	1.726	296.	3.3
AD264	NA	3.00	.798	1.745	296.	3.4
AD265	A	3.00	.810	1.745	296.	3.5
AD267	NA	3.00	.841	1.875	295.	3.8
AD268	A	3.00	.876	1.887	296.	3.9
AD269	NA	3.00	.799	1.685	296.	3.3
AD270	A	3.00	.806	1.689	294.	3.4
AD271	NA	8.00	.697	1.701	296.	3.1
AD272	A	8.00	.696	1.687	295.	3.1

TERMS FOR PAGE /16/:

1. canard aircraft (balance)
2. test
3. adaptive/non-adaptive
4. canard aircraft (pressure)

LIST OF FIGURES

CM

.029
.029
.031
.033
.033
.037
.037
.032
.033
.033
.033
.033
.033
.033
.032
.032
.033
.032
.033
.033
.032
.031
.031
.031
131
034
.033
.033
.034
.034

FIG. 1 - T2 wind tunnel.

FIG. 2 - CERT T2 test section - C5 body in the test section.

FIG. 3 - C5 model.

FIG. 4 - F4 model.

FIG. 5 - Mach number distribution along flexible wall with C5.

FIG. 6 - Mach number distribution along flexible walls model.

FIG. 7 - Flexible walls shapes with C5 model.

FIG. 8 - Mach number distribution around C5 model.

FIG. 9 - Mach number distribution around canard model.

FIG. 10 - C5 model Mach number distribution (M_o = 0.6, 0.7, 0.84).

FIG. 11 - C5 model Mach number distribution (M_o > 0.8).

FIG. 12 - Comparison between TuB and T2, results at M_o = 0.7.

FIG. 13 - Comparison between TuB and T2, results at M_o = 0.84.

FIG. 14 - Comparison between NASA Ames and T2, results at M_o = 0.7.

FIG. 15 - Comparison between NASA Ames and T2, results at M_o = 0.84.

FIG. 16 - Comparison between NASA Ames and T2, results at M_o = 0.95.

FIG. 17 - Comparison between NASA Ames and T2, results at M_o = 0.97.

FIG. 18 - Comparison between calculation and experiment on C5 model.

FIG. 19 - Comparison between calculation and experiment around C5 model and its sting.

FIG. 20 - Mach number distribution along flexible walls with F4 model.

FIG. 21 - F4 model, lift, drag and pitching moment, M = 0.7.

FIG. 22 - Canard model lift coefficient.

FIG. 23 - Canard model, lift, drag and pitching moment, M = 0.7.

FIG. 24 - Canard model lift coefficinet - M_o effect.

FIG. 25 - Canard model lift coefficient versus M_o.

FIG. 26 - Mach number distribution along flexible walls with canard model.

FIG. 27 - Mach number distribution on the canard model (M_o = 0.7).

FIG. 28 - Adaptation effect on the canard model Mach number distribution (M_o = 0.7, α = 0.8°).

FIG. 29 - Mach number distribution along flexible walls with the canard model.

FIG. 30 - Flexible wall shapes around tha canard model.

FIG. 31 - Mach number distribution on the canard model (M_o effect).

FIG. 32 - Nominal and real (balance or forto) angle of attack with the canard model.

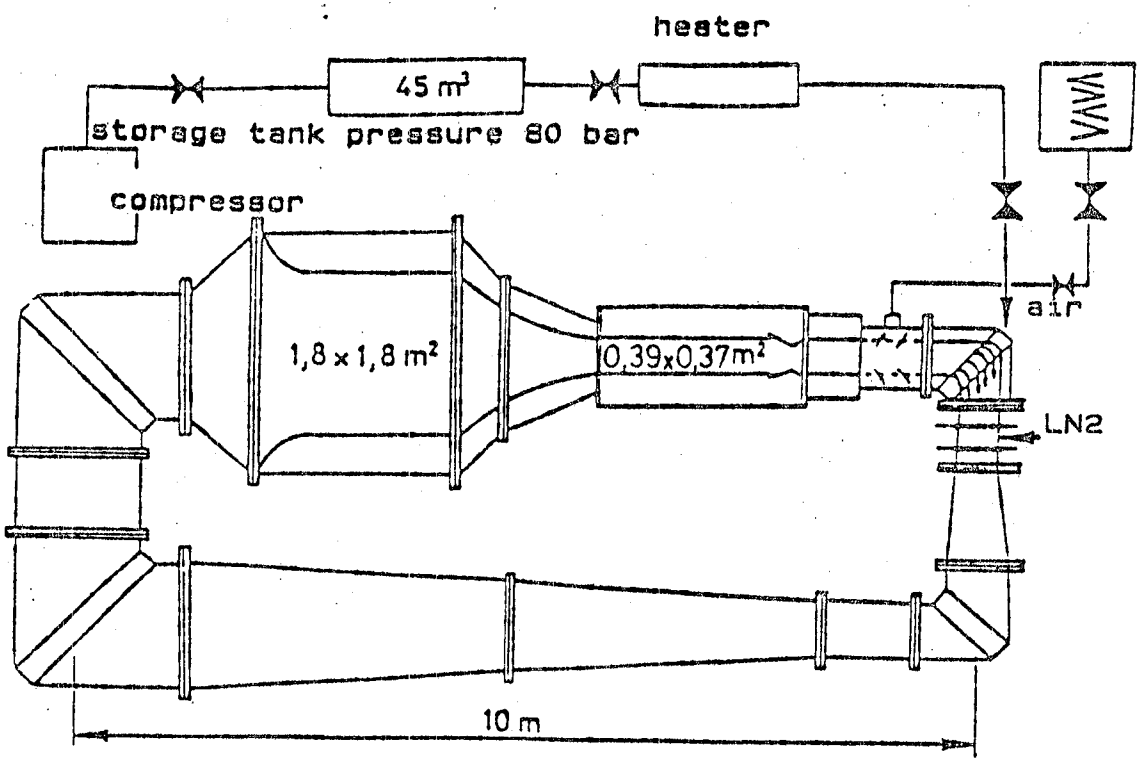

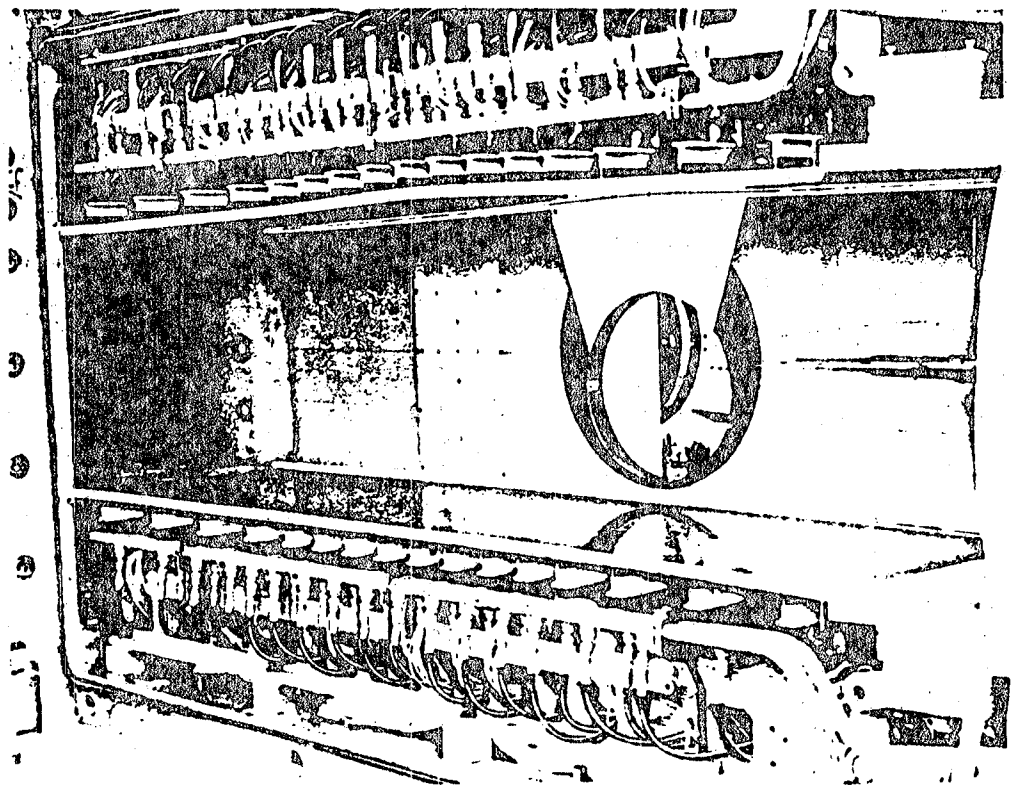

FIG 1: T2 WIND TUNNEL - ADAPTIVE WALL TEST SECTION

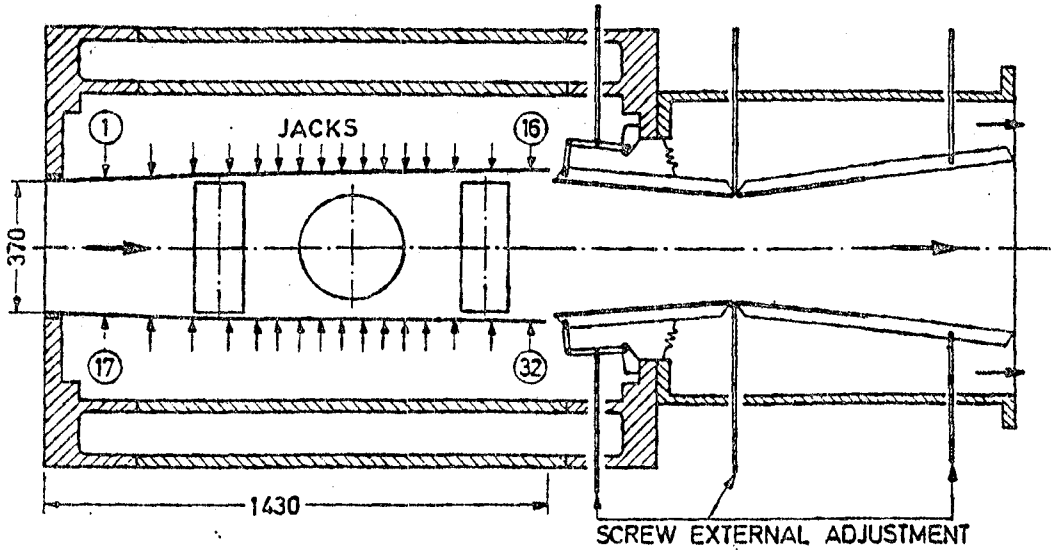

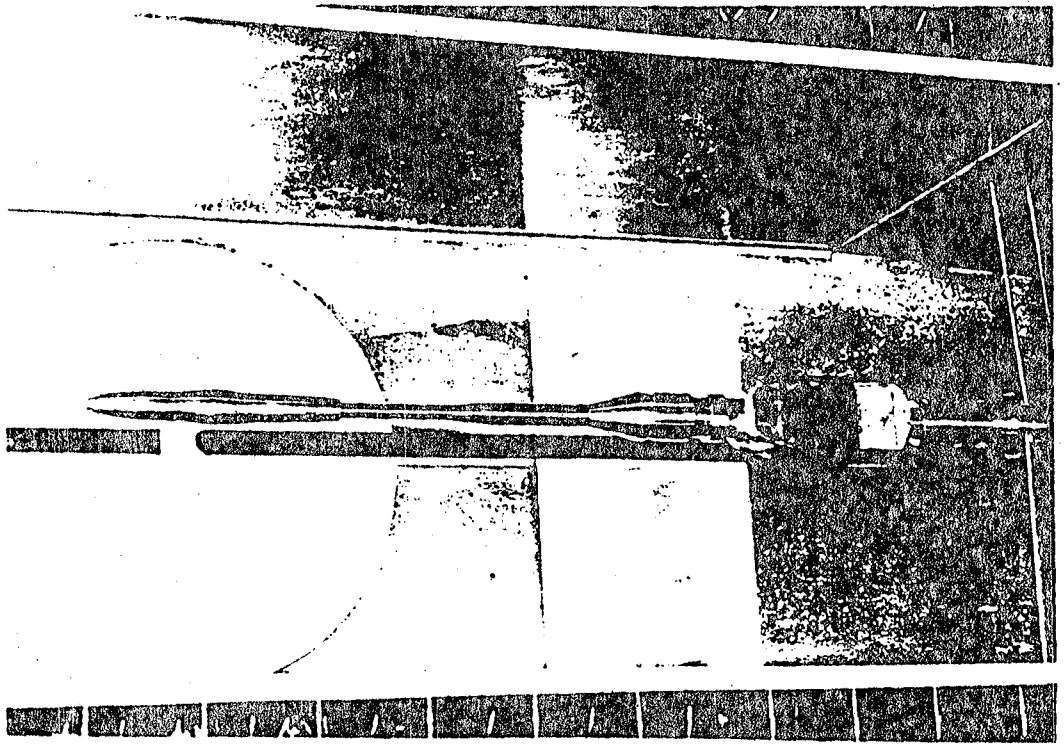

FIG 2: T2 TEST SECTION - C5 MODEL IN THE TEST SECTION

Position of pressure holes

N°	1	2	3	4	5	6	7	8	9	10	11	12	13	14	15	16	17	18	19	20
X (mm)	0	6	22	39	47	61	77	85	88	91	96	100	106	116	132	142	154	159	163	166.28

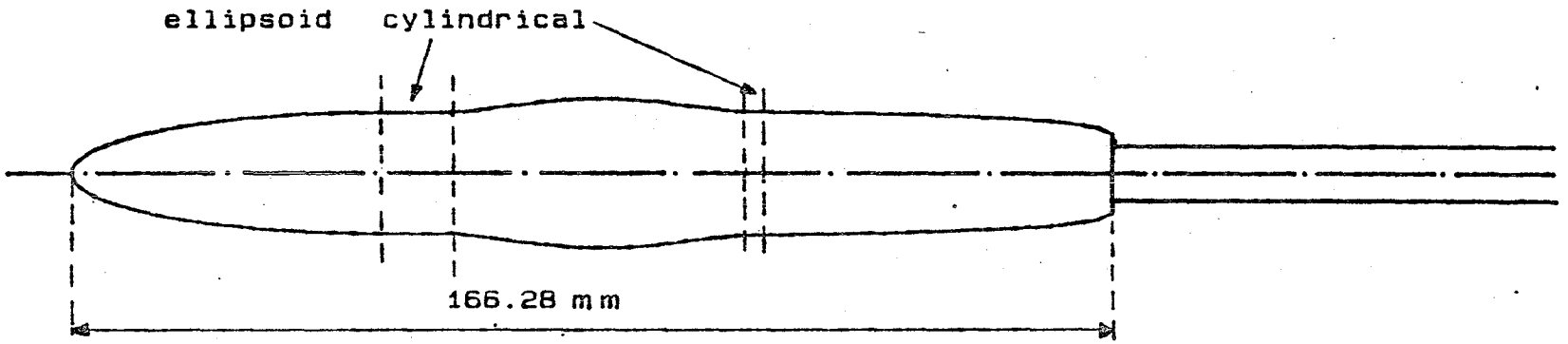

FIG 3: C5 MODEL

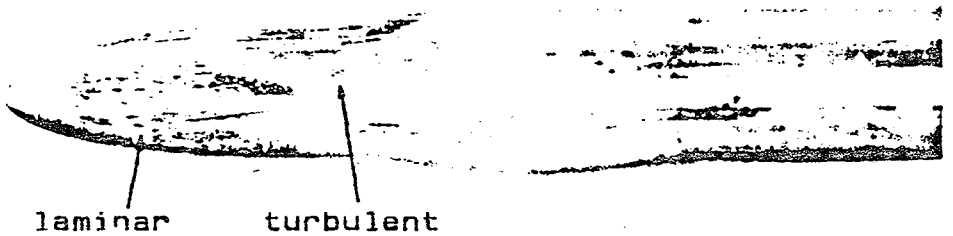

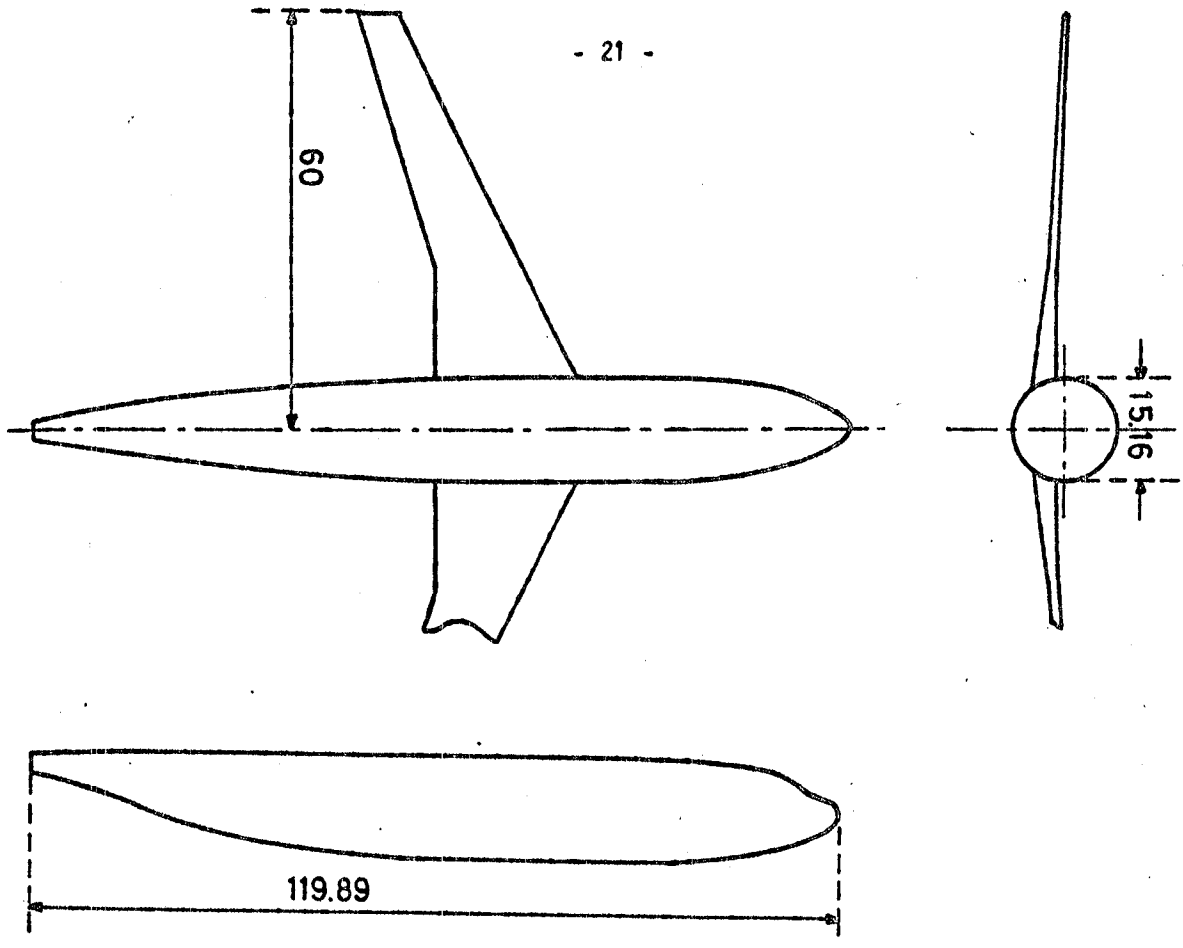

FIG 4: F4 MODEL

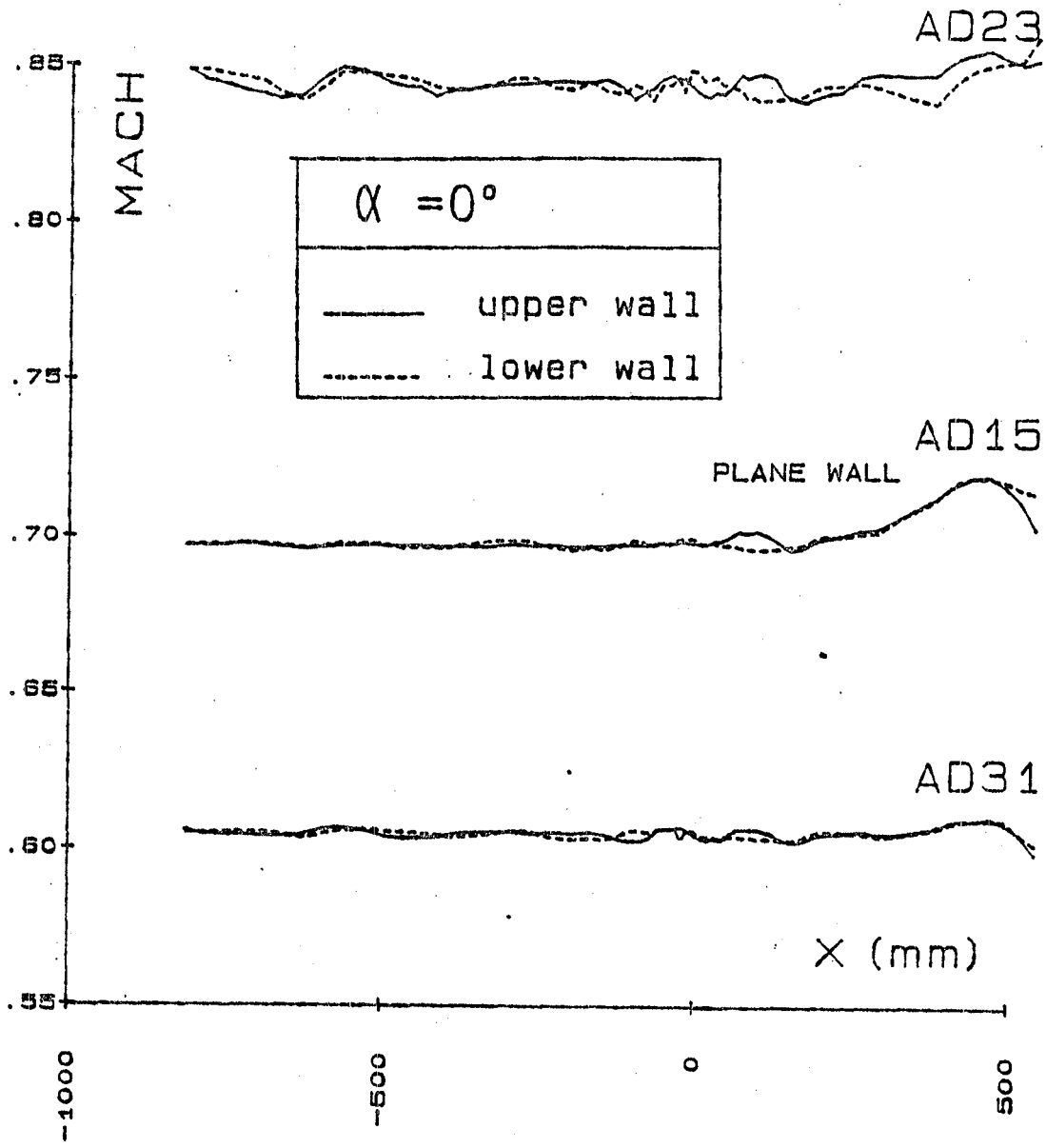

FIG 5: MACH NUMBER DISTRIBUTION ALONG FLEXIBLE WALLS WITH C5 MODEL

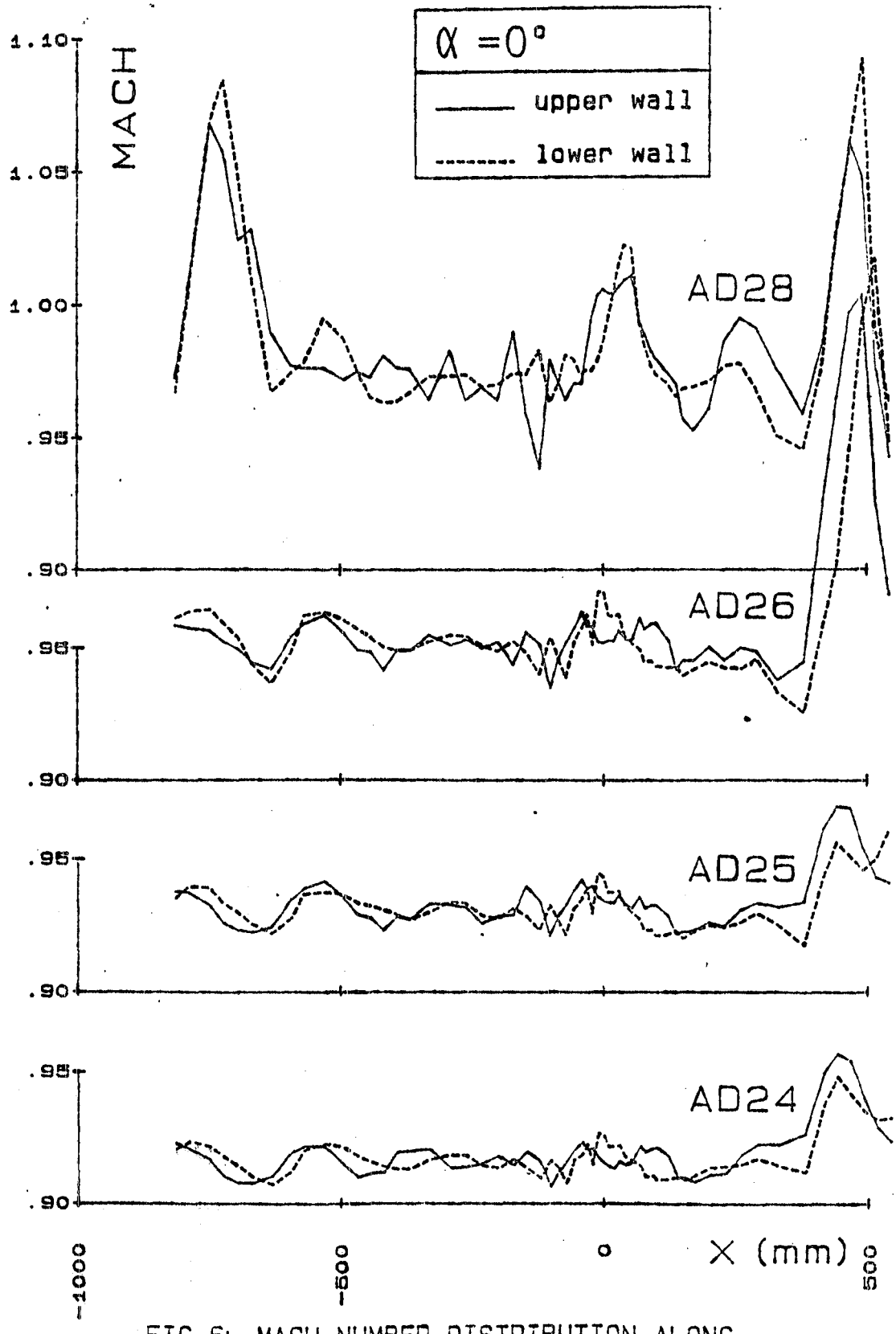

FIG 6: MACH NUMBER DISTRIBUTION ALONG FLEXIBLE WALLS WITH C5 MODEL

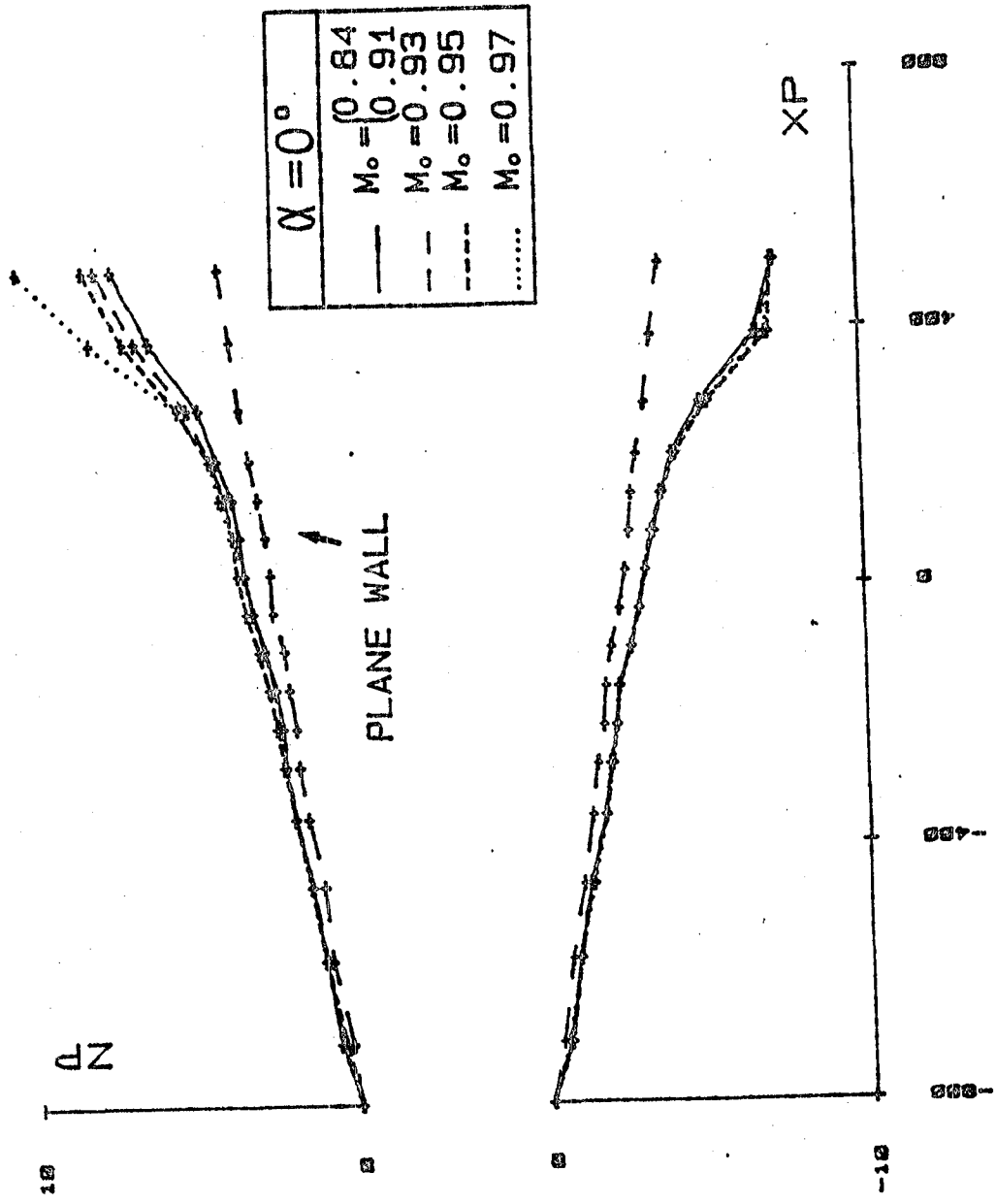

FIG 7: FLEXIBLE WALL SHAPES WITH C5 MODEL

FIG 7: FLEXIBLE WALL SHAPES WITH C5 MODEL

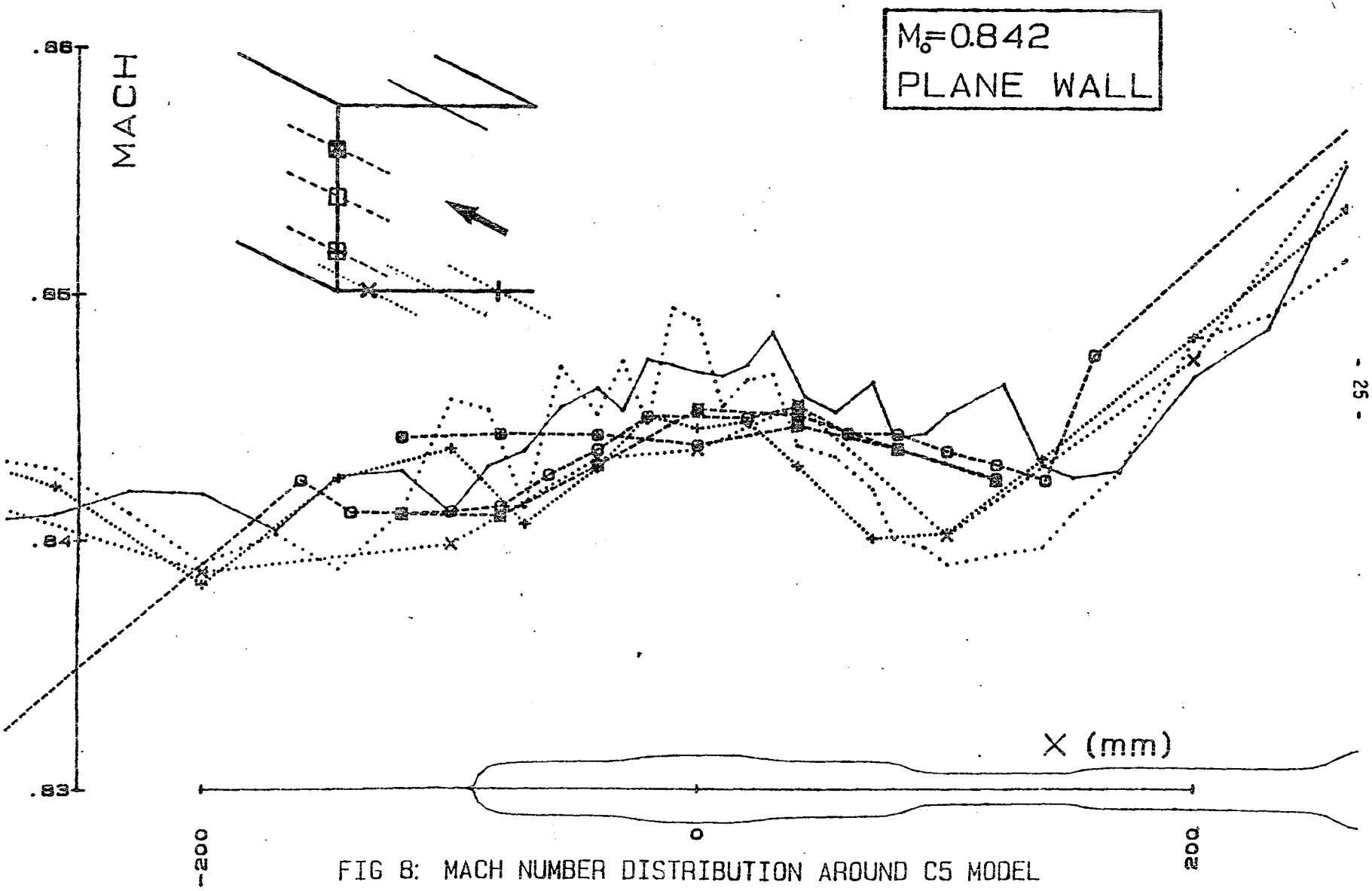

FIG 8: MACH NUMBER DISTRIBUTION AROUND C5 MODEL

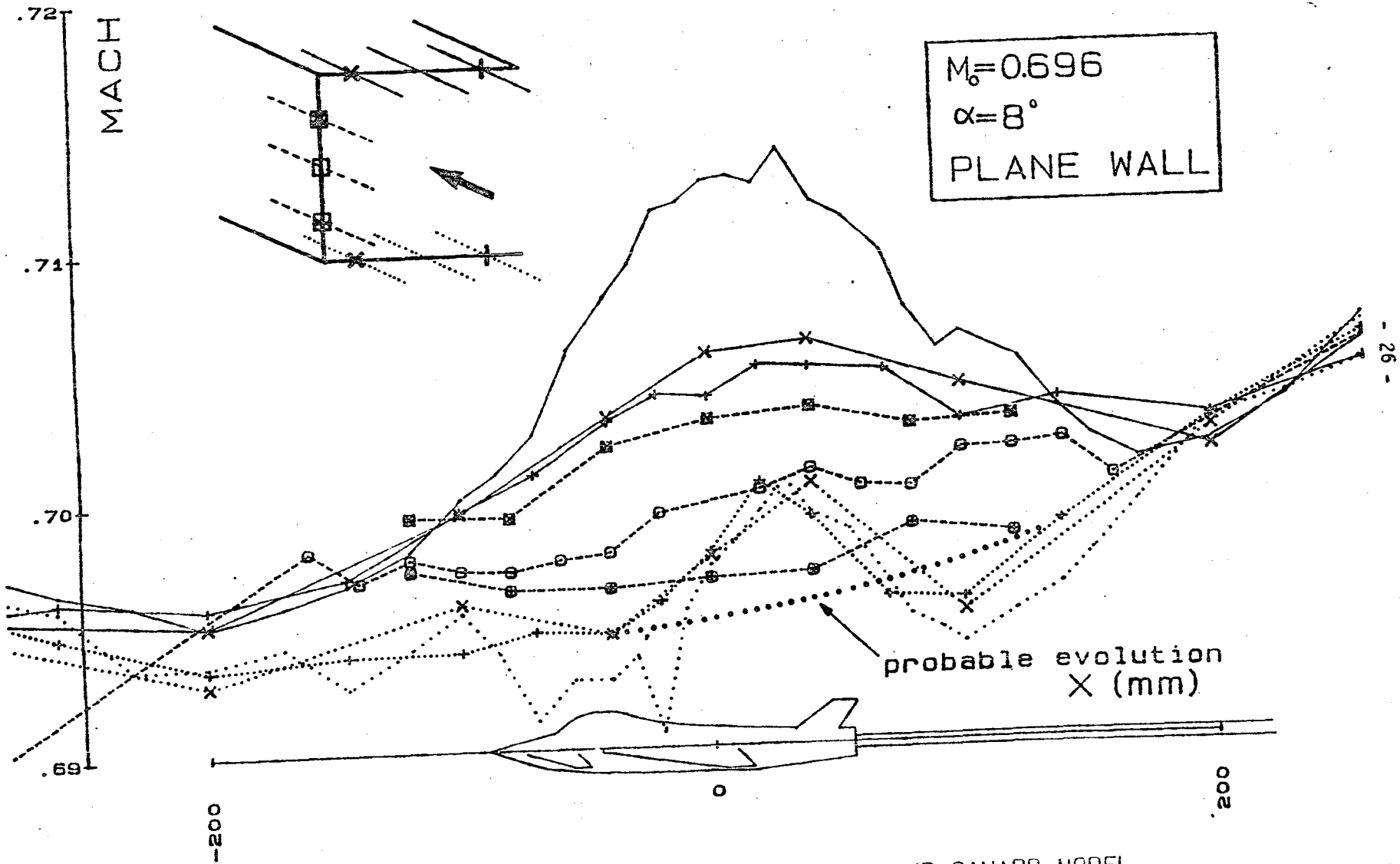

FIG 9: MACH NUMBER DISTRIBUTION AROUND CANARD MODEL

-200 0 200

FIG 9: MACH NUMBER DISTRIBUTION AROUND CANARD MODEL

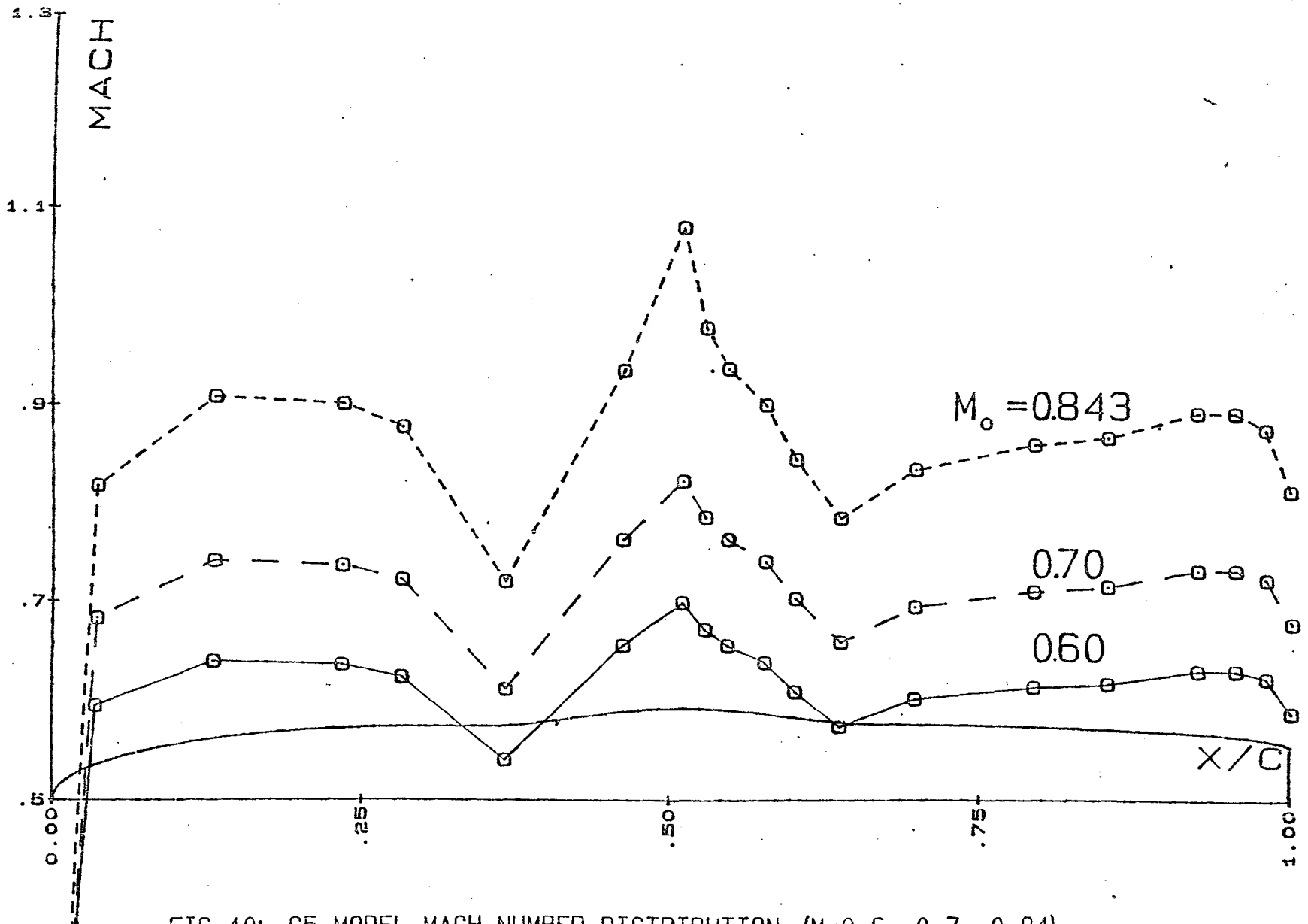

FIG 10: C5 MODEL MACH NUMBER DISTRIBUTION (M_o=0.6, 0.7, 0.84)

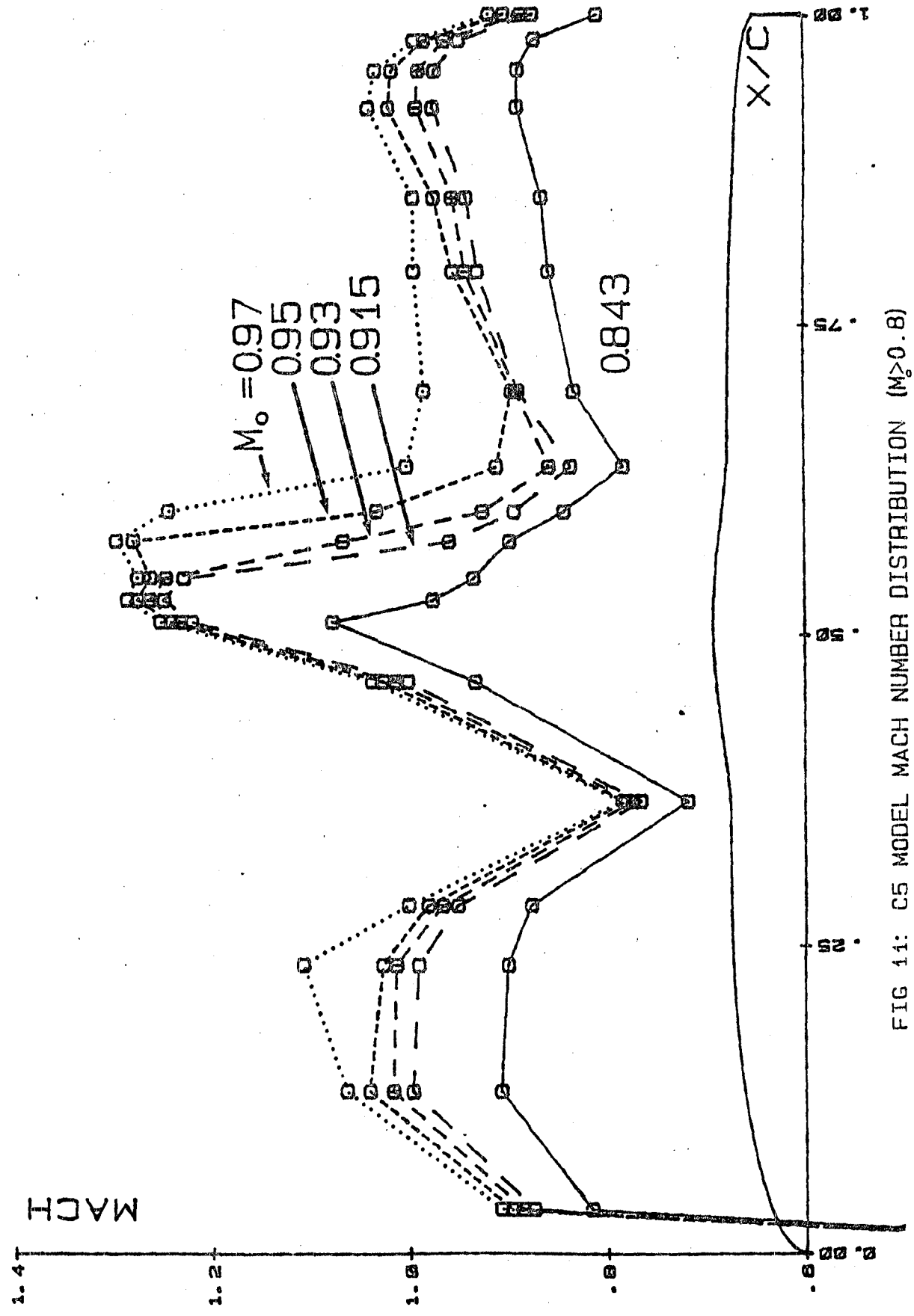

FIG 11: C5 MODEL MACH NUMBER DISTRIBUTION (M_o>0.8)

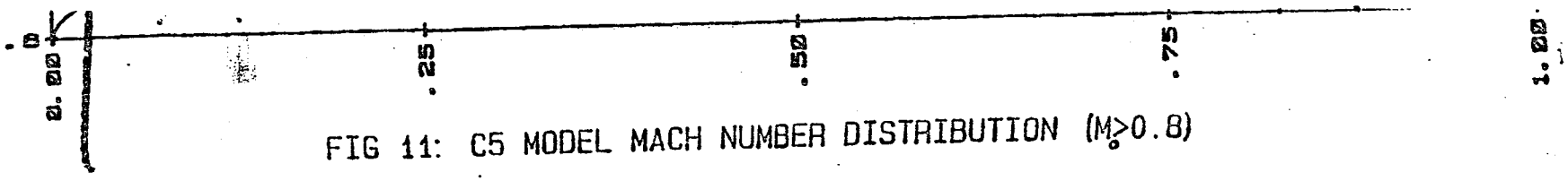

FIG 11: C5 MODEL MACH NUMBER DISTRIBUTION (M_∞>0.8)

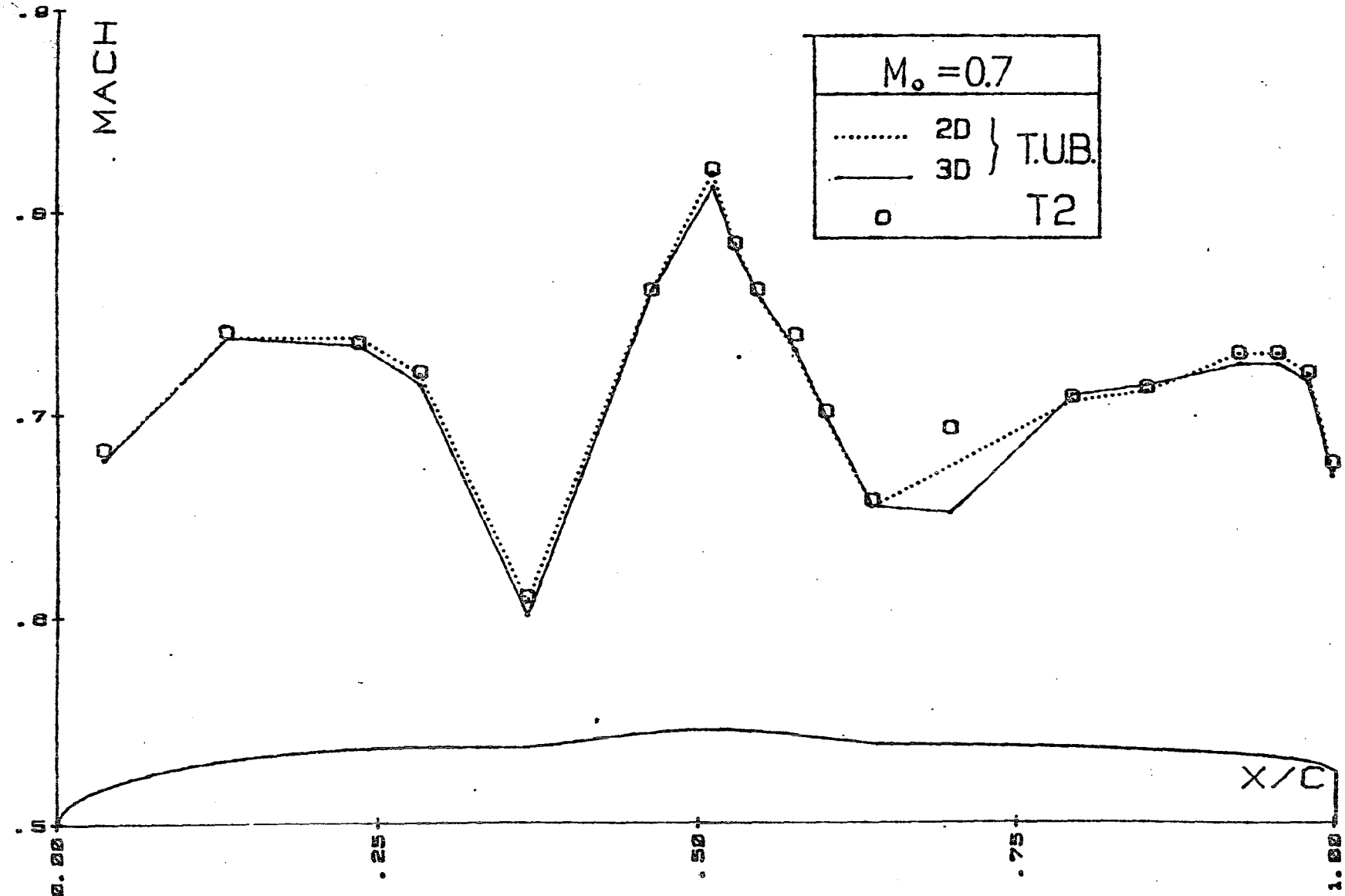

FIG 12: COMPARISON BETWEEN TUB AND T2 RESULTS AT M_∞=0.7

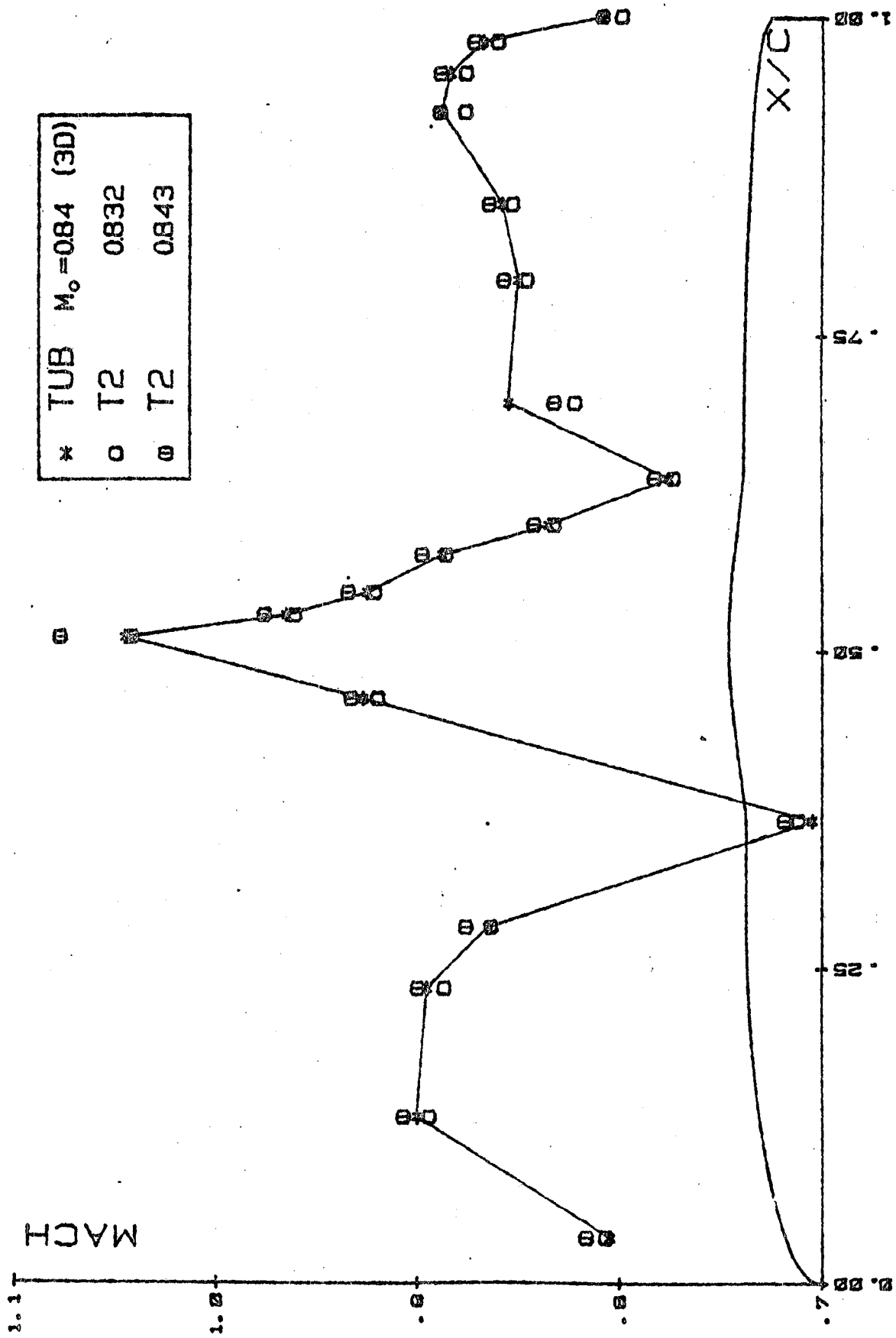

FIG 13: COMPARISON BETWEEN TUB AND T2 RESULTS AT M_∞=0.84

FIG 13: COMPARISON BETWEEN TUB AND T2 RESULTS AT M_o=0.84

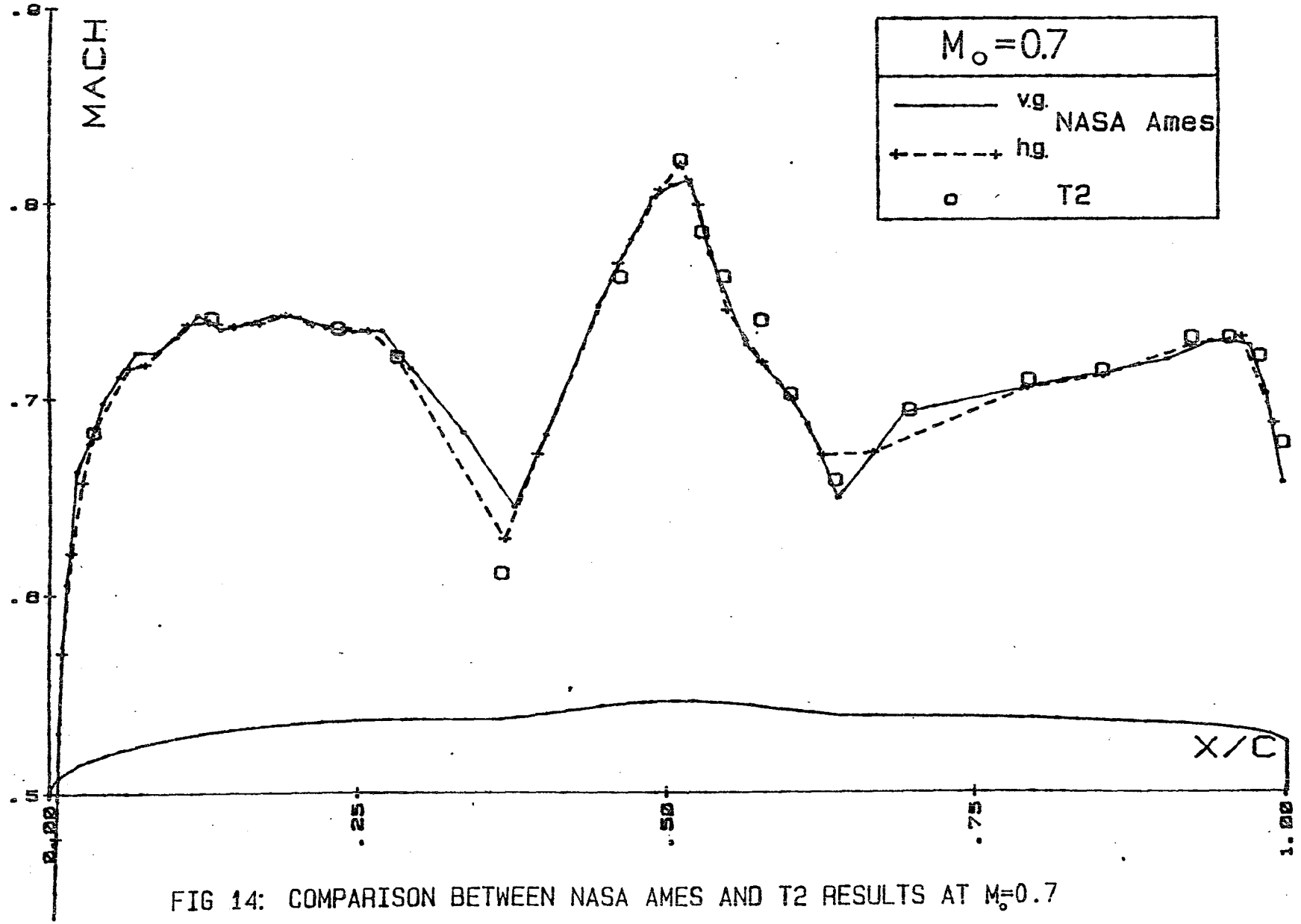

FIG 14: COMPARISON BETWEEN NASA AMES AND T2 RESULTS AT M_o=0.7

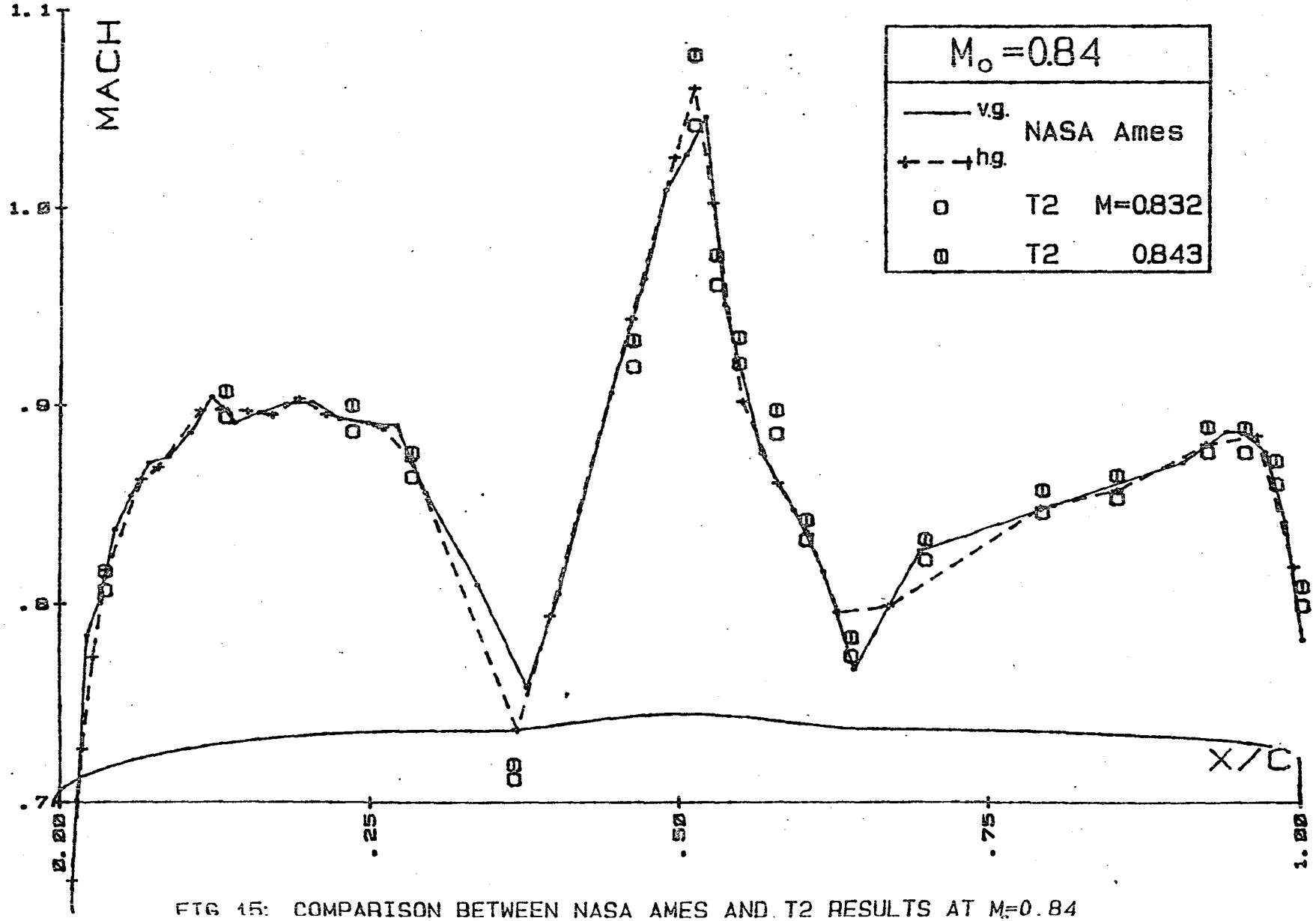

FIG 15: COMPARISON BETWEEN NASA AMES AND T2 RESULTS AT M_∞=0.84

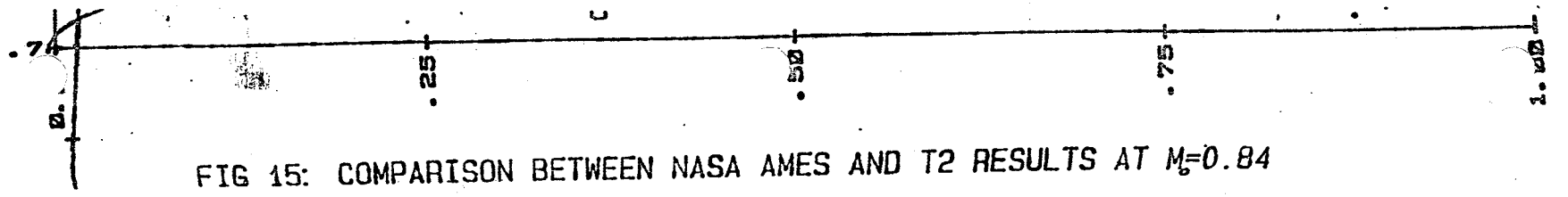

FIG 15: COMPARISON BETWEEN NASA AMES AND T2 RESULTS AT M_o=0.84

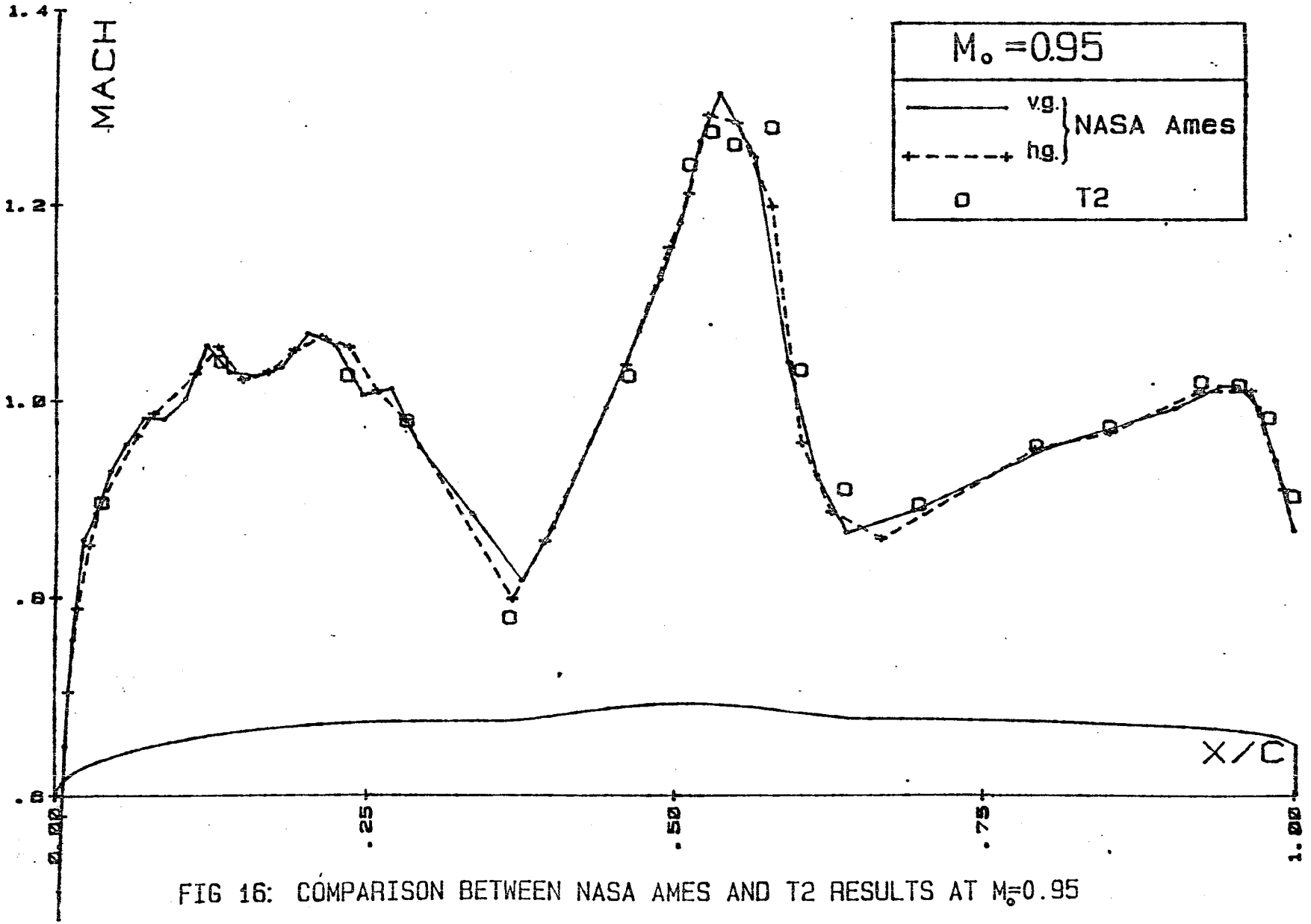

FIG 16: COMPARISON BETWEEN NASA AMES AND T2 RESULTS AT M_o=0.95

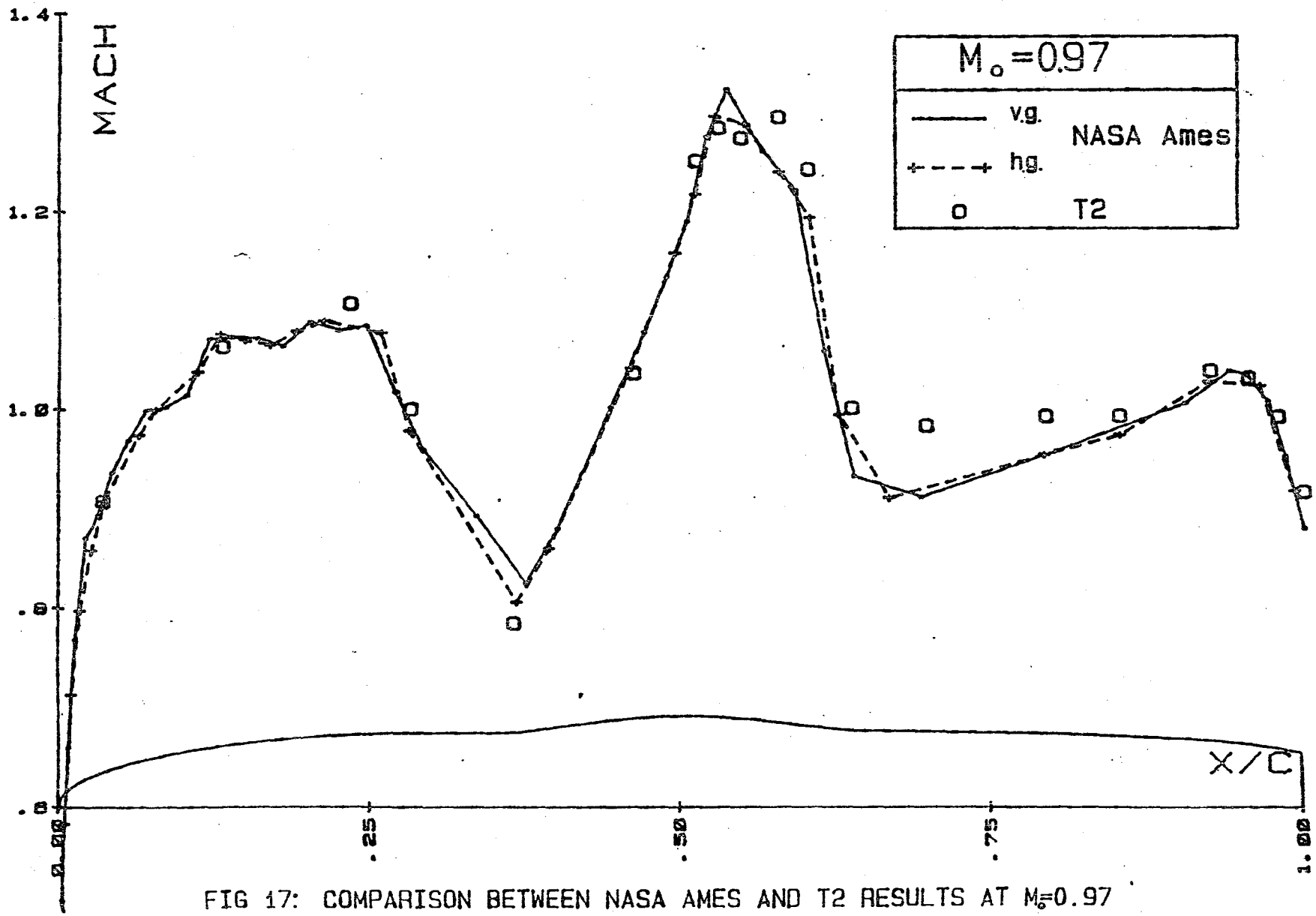

FIG 17: COMPARISON BETWEEN NASA AMES AND T2 RESULTS AT M_o=0.97

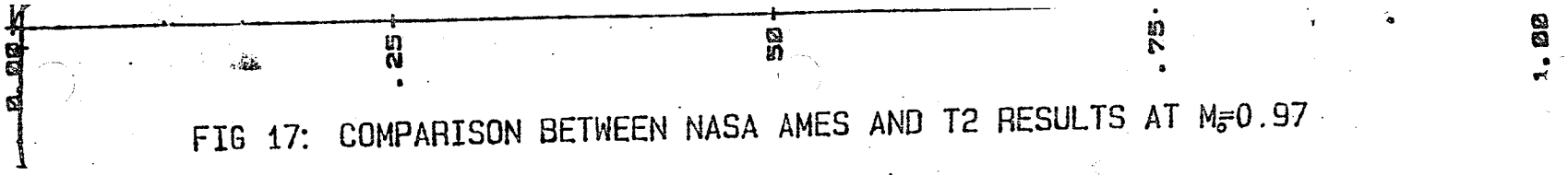

FIG 17: COMPARISON BETWEEN NASA AMES AND T2 RESULTS AT M_∞=0.97

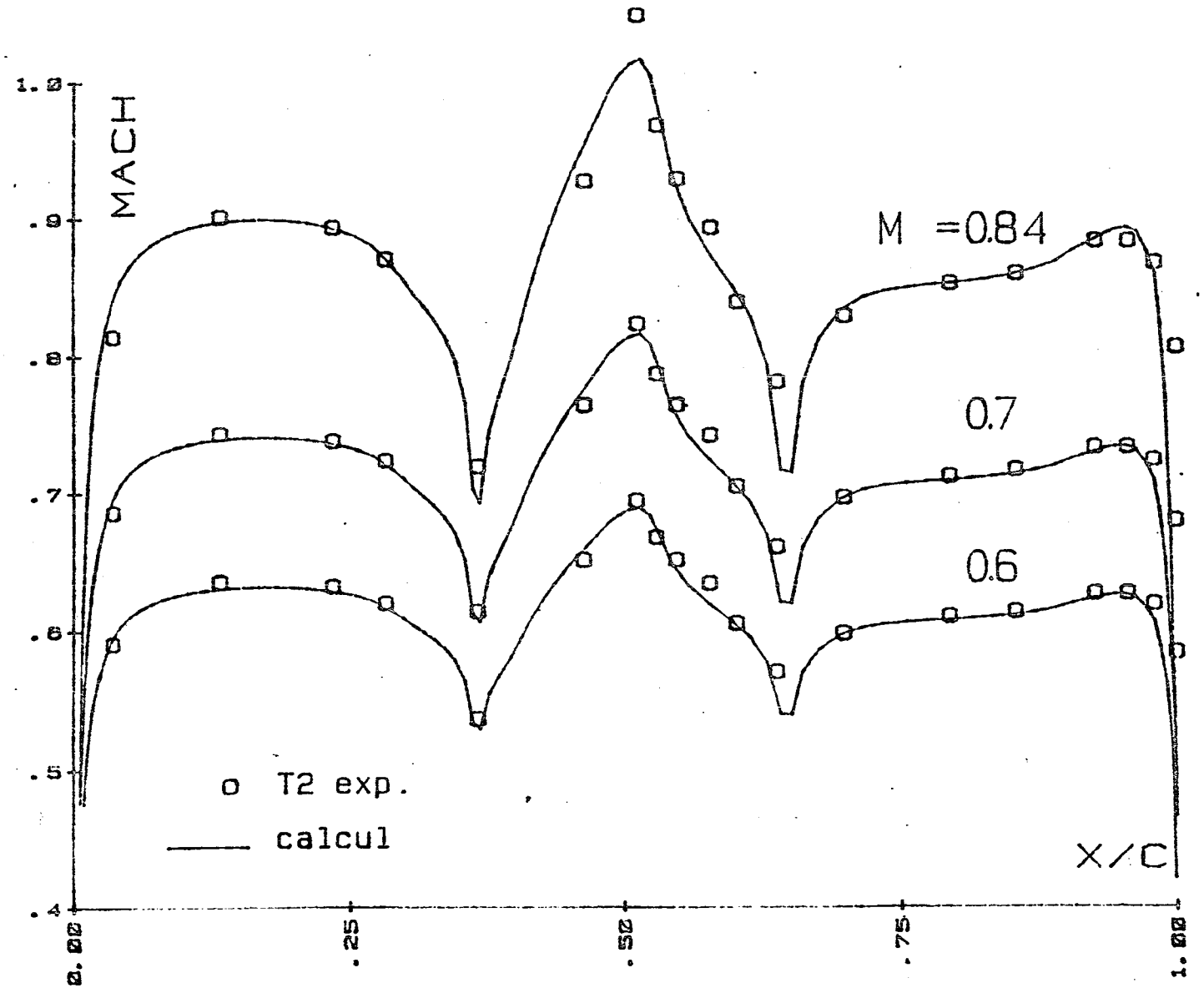

FIG 18: COMPARISON BETWEEN CALCULATION AND EXPERIMENT ON C5 MODEL

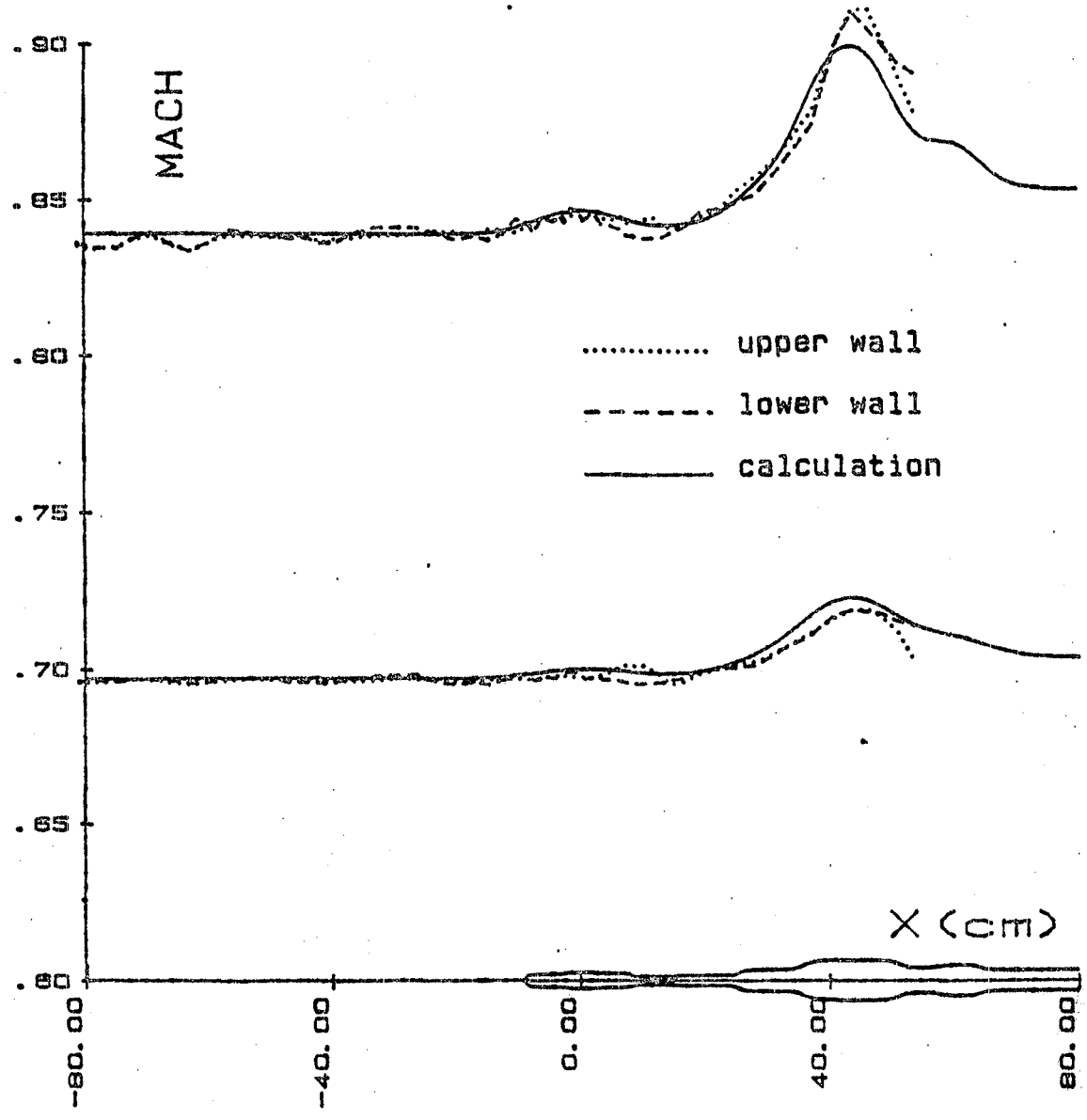

FIG 19: COMPARISON BETWEEN CALCULATION AND EXPERIMENT AROUND C5 MODEL AND ITS STING

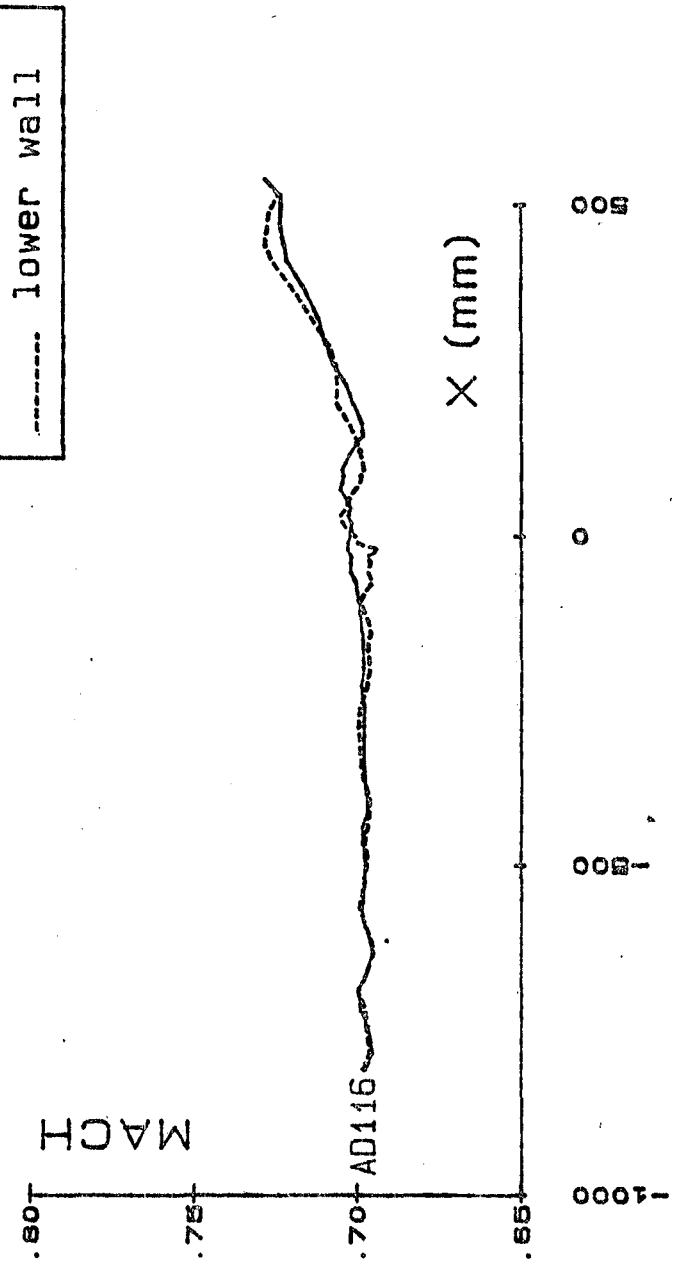

FIG 20: MACH NUMBER DISTRIBUTION ALONG FLEXIBLE WALLS WITH F4 MODEL

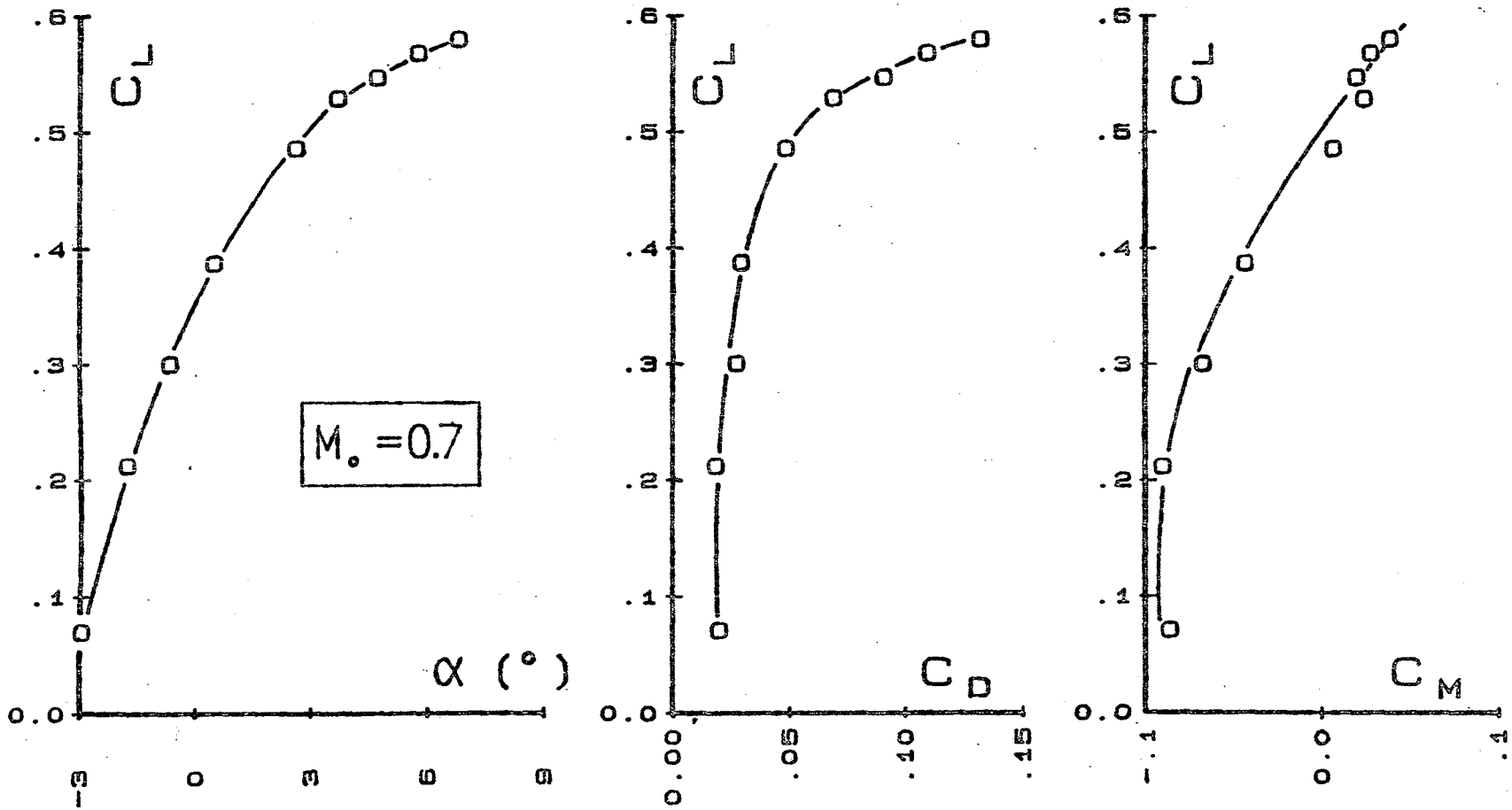

FIG 21: F4 MODEL, LIFT, DRAG AND PITCHING MOMENT, M_∞=0.7

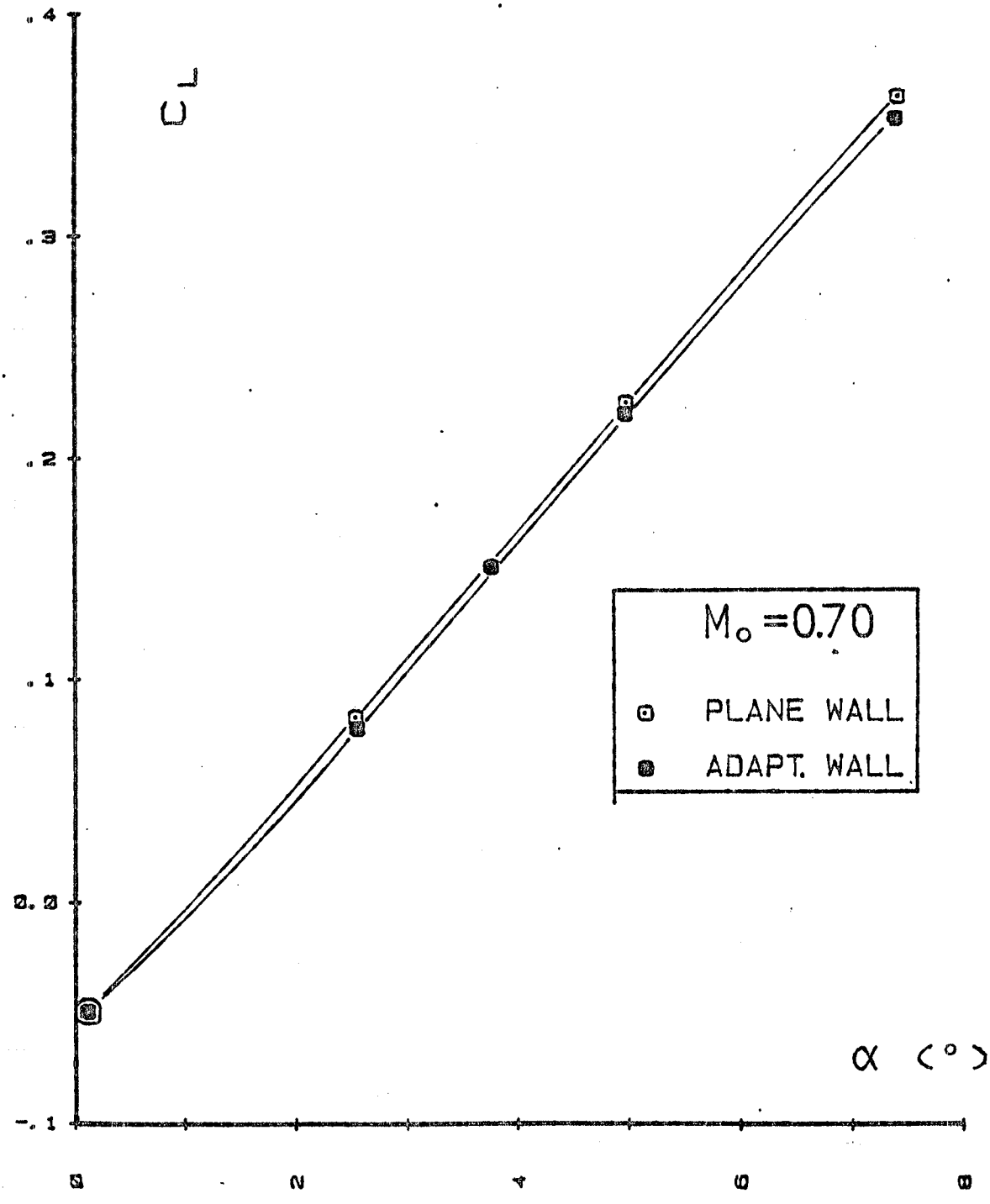

FIG 22: CANARD MODEL LIFT COEFFICIENT

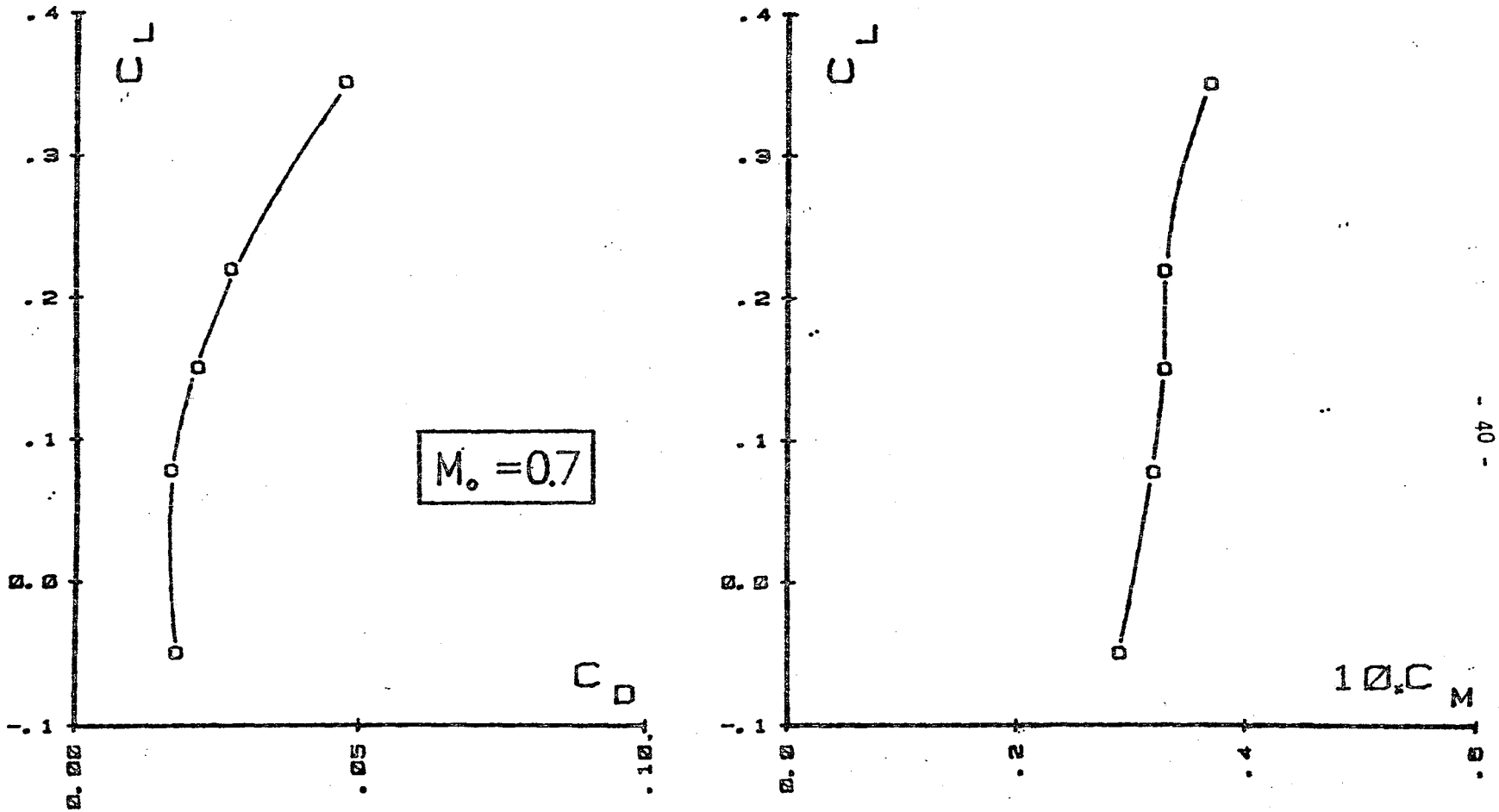

FIG 23: CANARD MODEL, LIFT, DRAG AND PITCHING MOMENT, M_o=0.7

FIG 23: CANARD MODEL, LIFT, DRAG AND PITCHING MOMENT, M_o=0.7

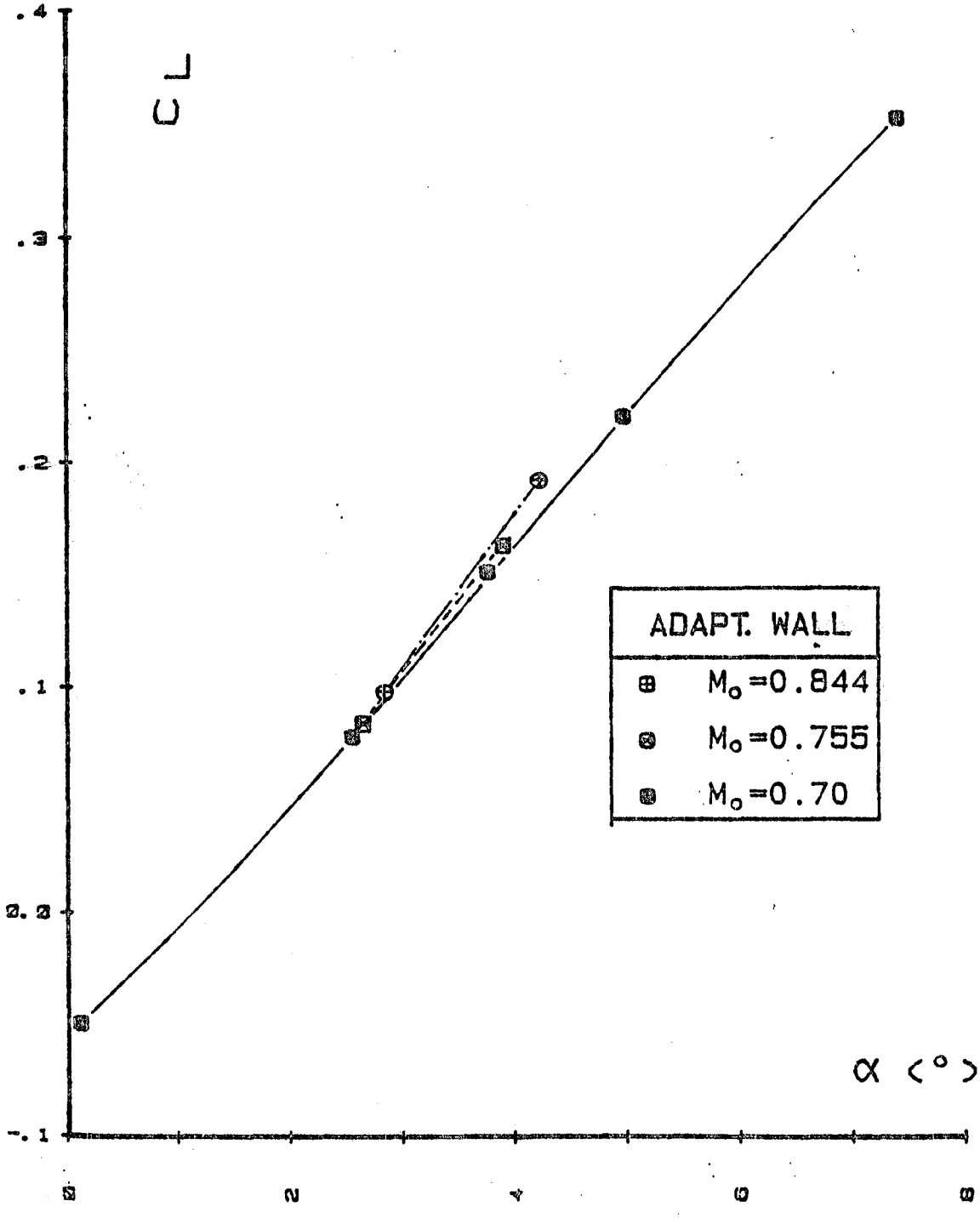

FIG 24: CANARD MODEL LIFT COEFFICIENT - M_o EFFECT

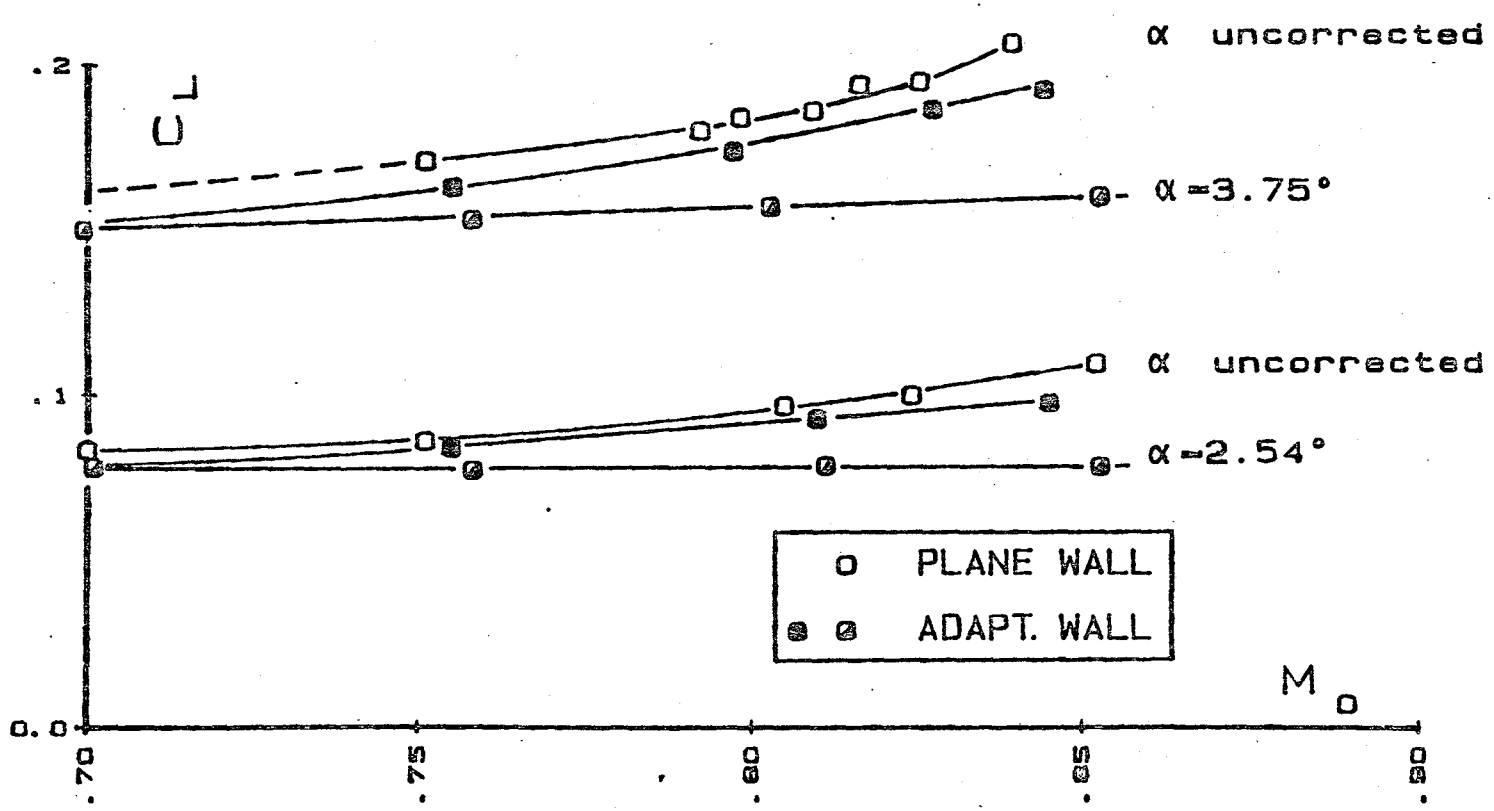

FIG 25: CANARD MODEL LIFT COEFFICIENT VERSUS M_o

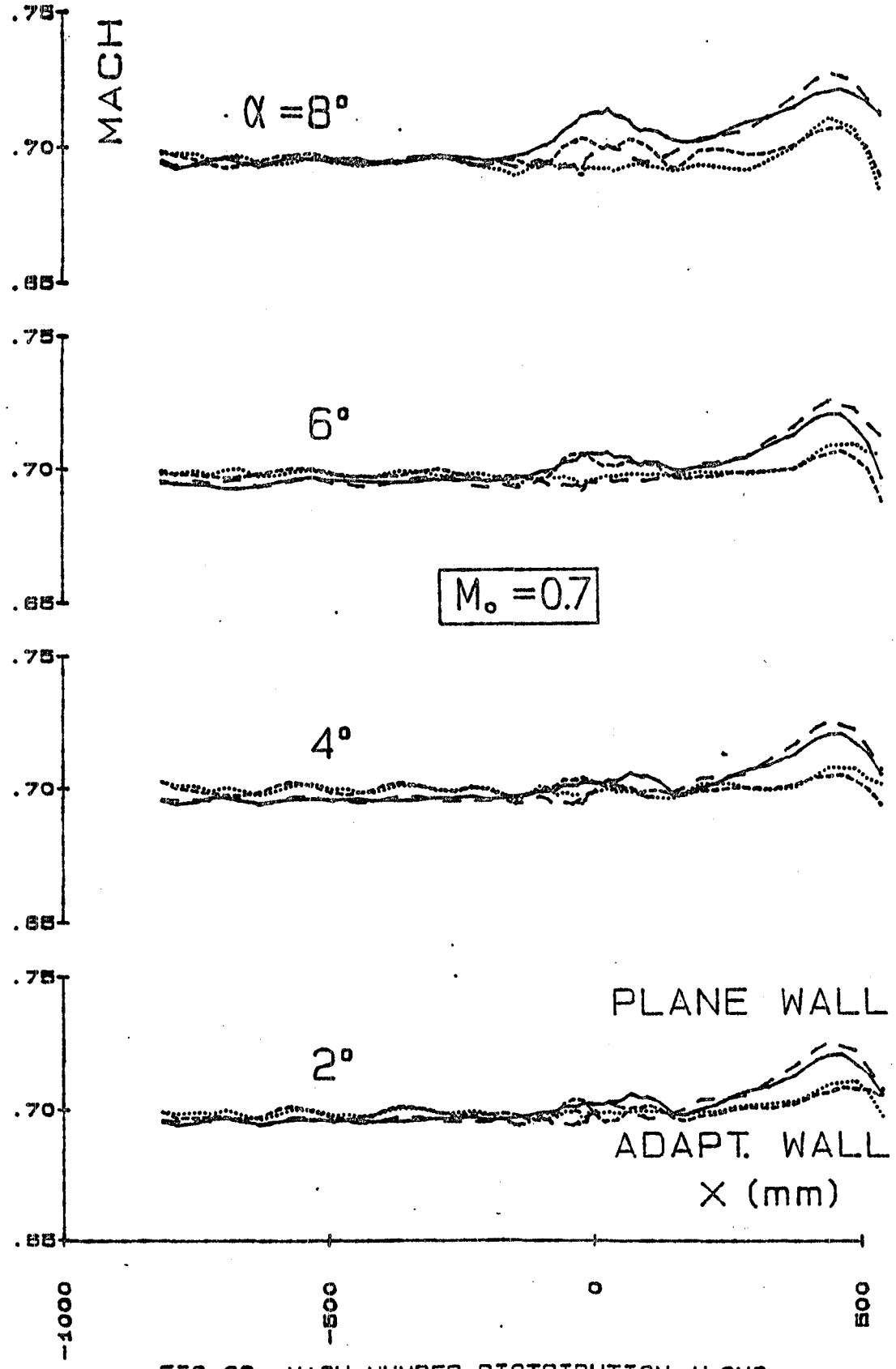

FIG 25: CANARD MODEL LIFT DISTRIBUTION VERSUS Mo

FIG 26: MACH NUMBER DISTRIBUTION ALONG FLEXIBLE WALLS WITH CANARD MODEL

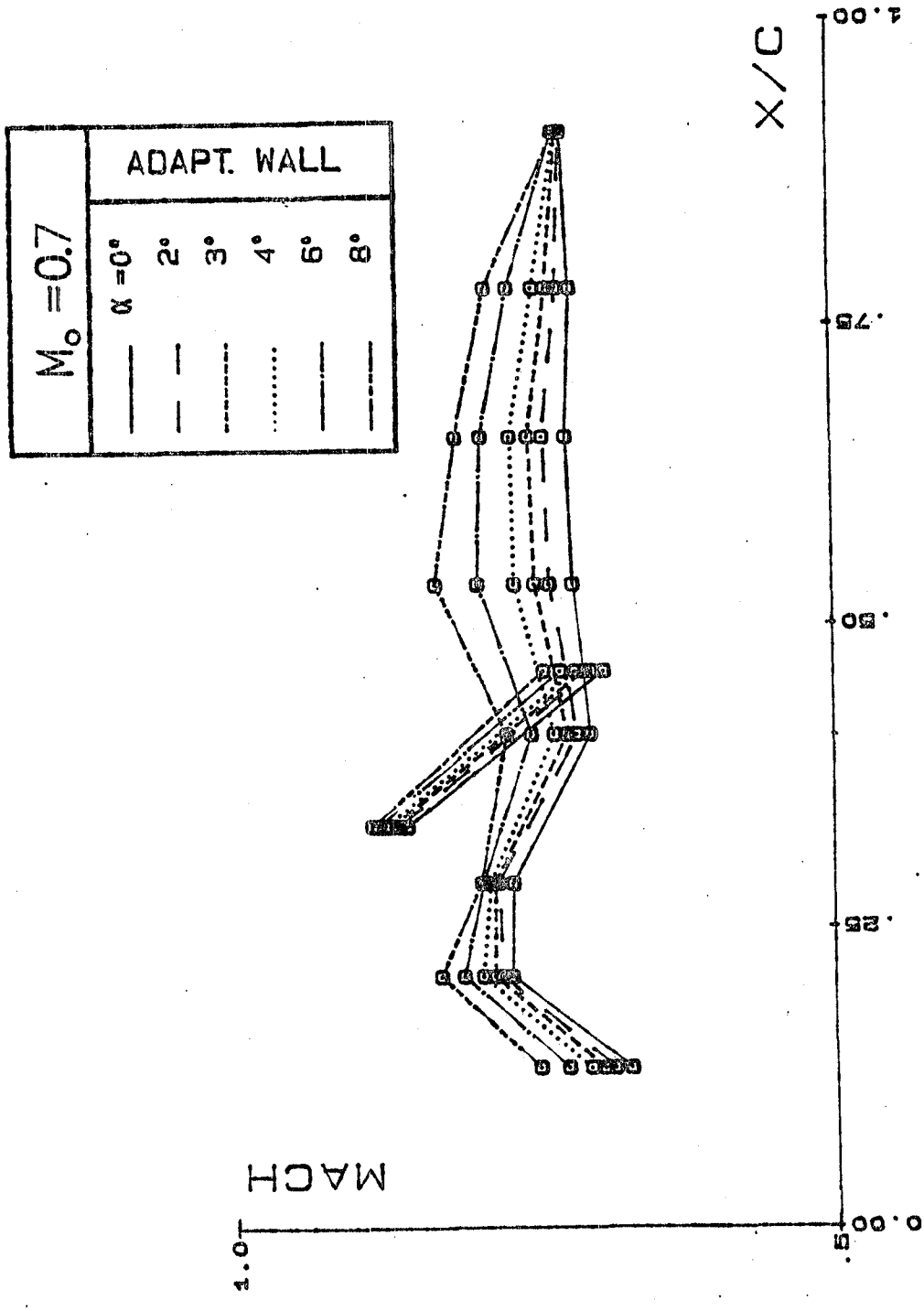

FIG 27: MACH NUMBER DISTRIBUTION ON THE CANARD MODEL (M_o=07)

FIG 27: MACH NUMBER DISTRIBUTION ON THE CANARD MODEL (M_o=07)

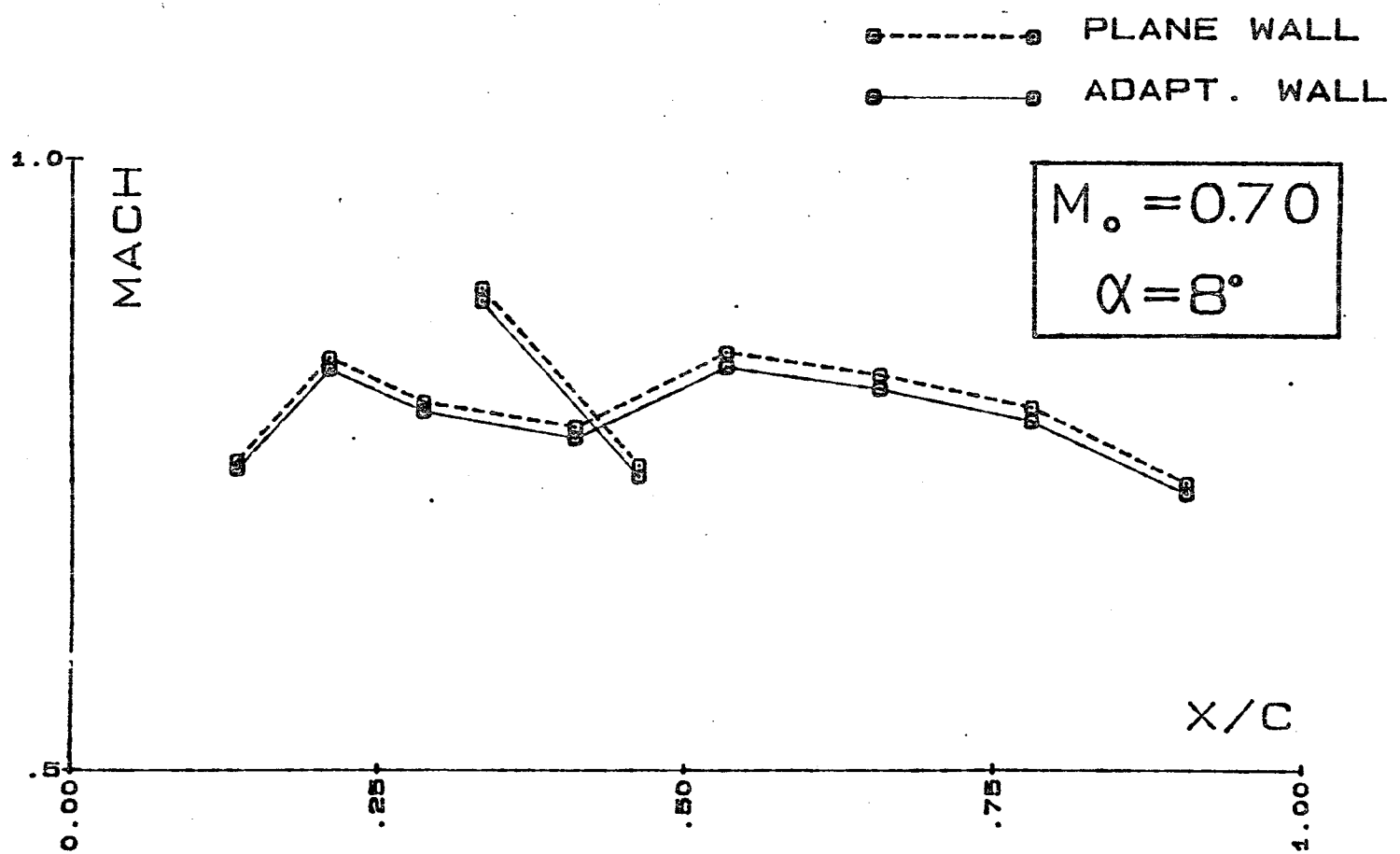

FIG 28: ADAPTATION EFFECT ON THE CANARD MODEL MACH NUMBER DISTRIBUTION (M_o=07, α =8°)

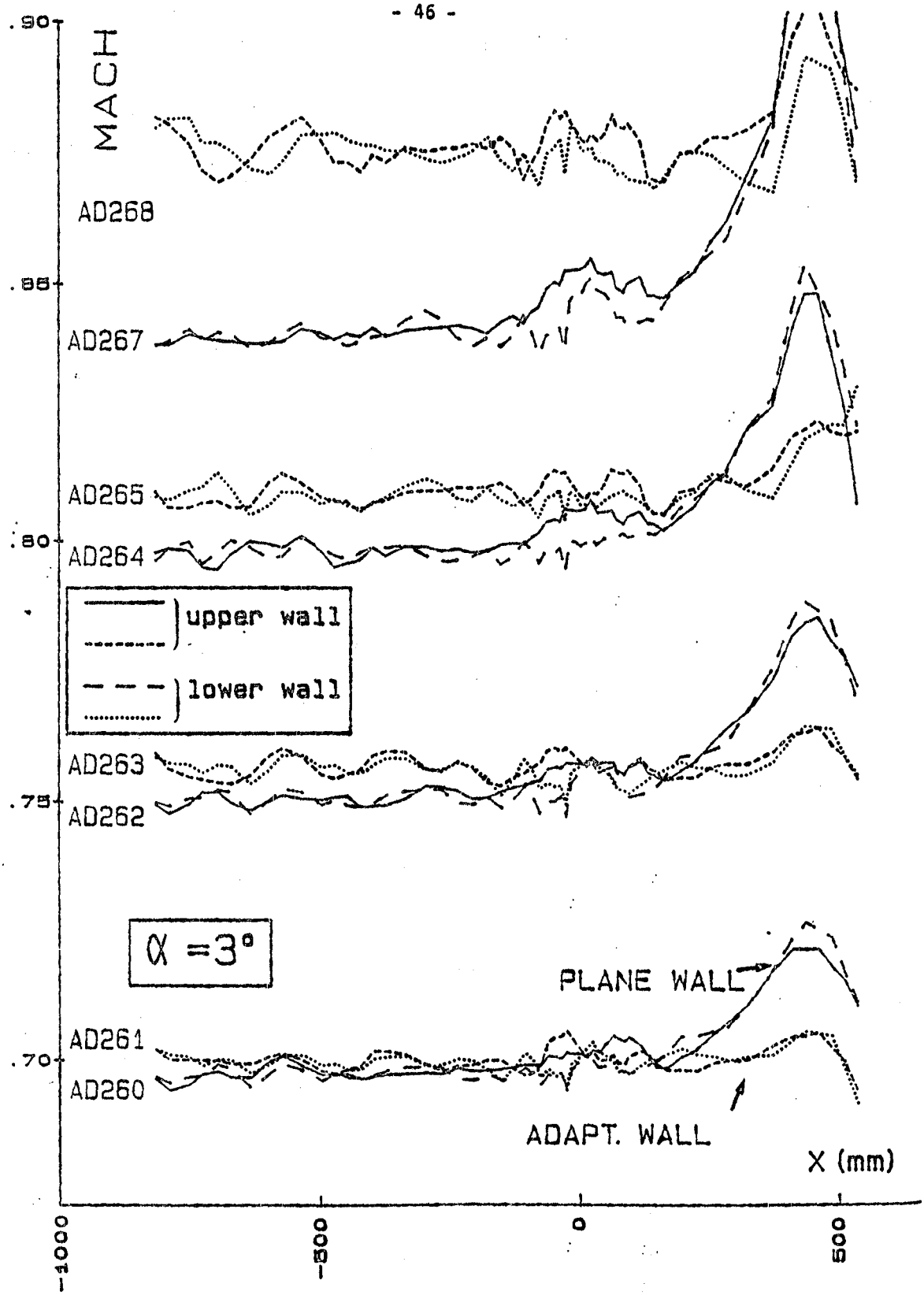

FIG 29: MACH NUMBER DISTRIBUTION ALONG FLEXIBLE WALLS WITH THE CANARD MODEL

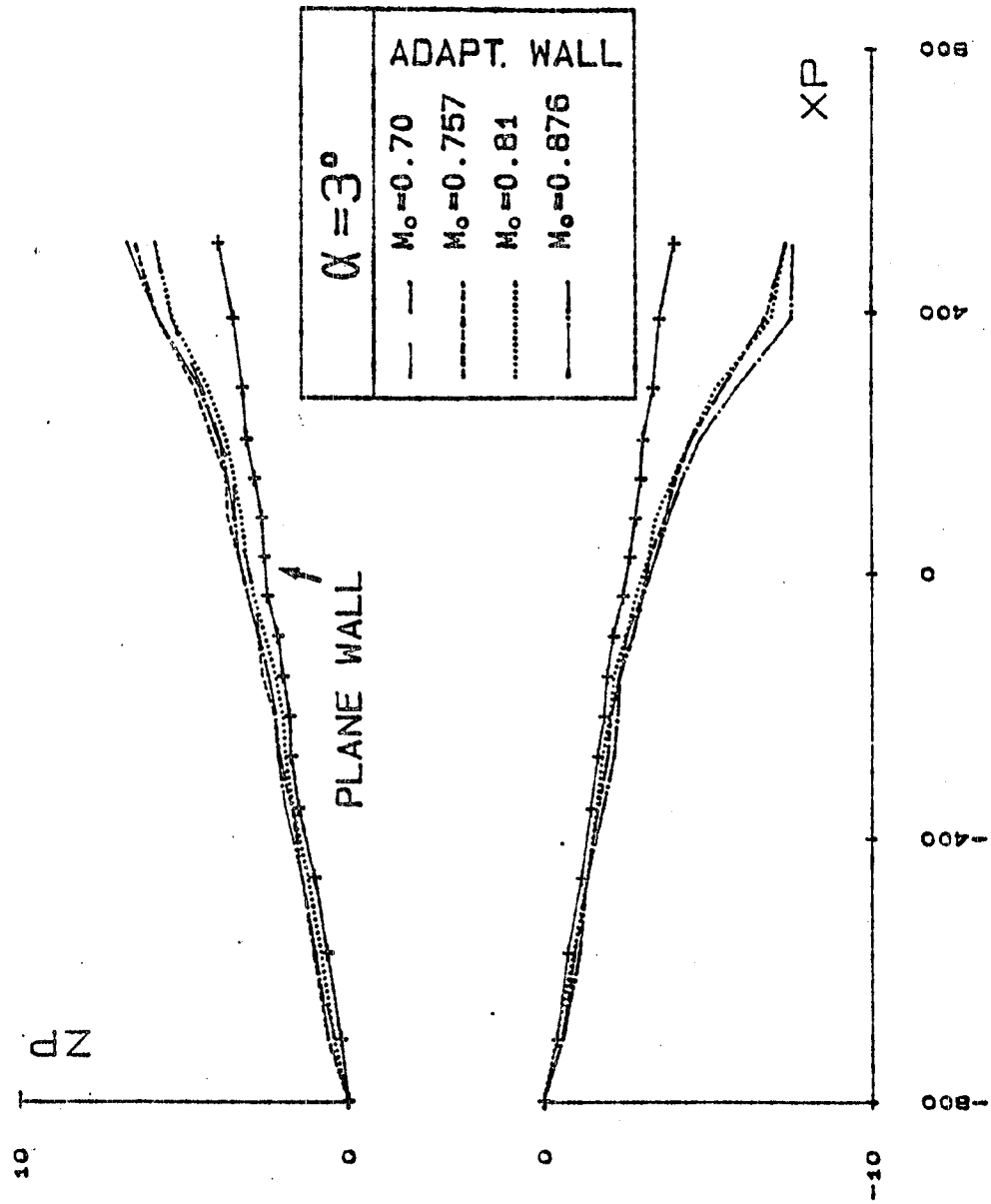

FIG 30: FLEXIBLE WALL SHAPES AROUND THE CANARD MODEL

X (mm)

500

LL3

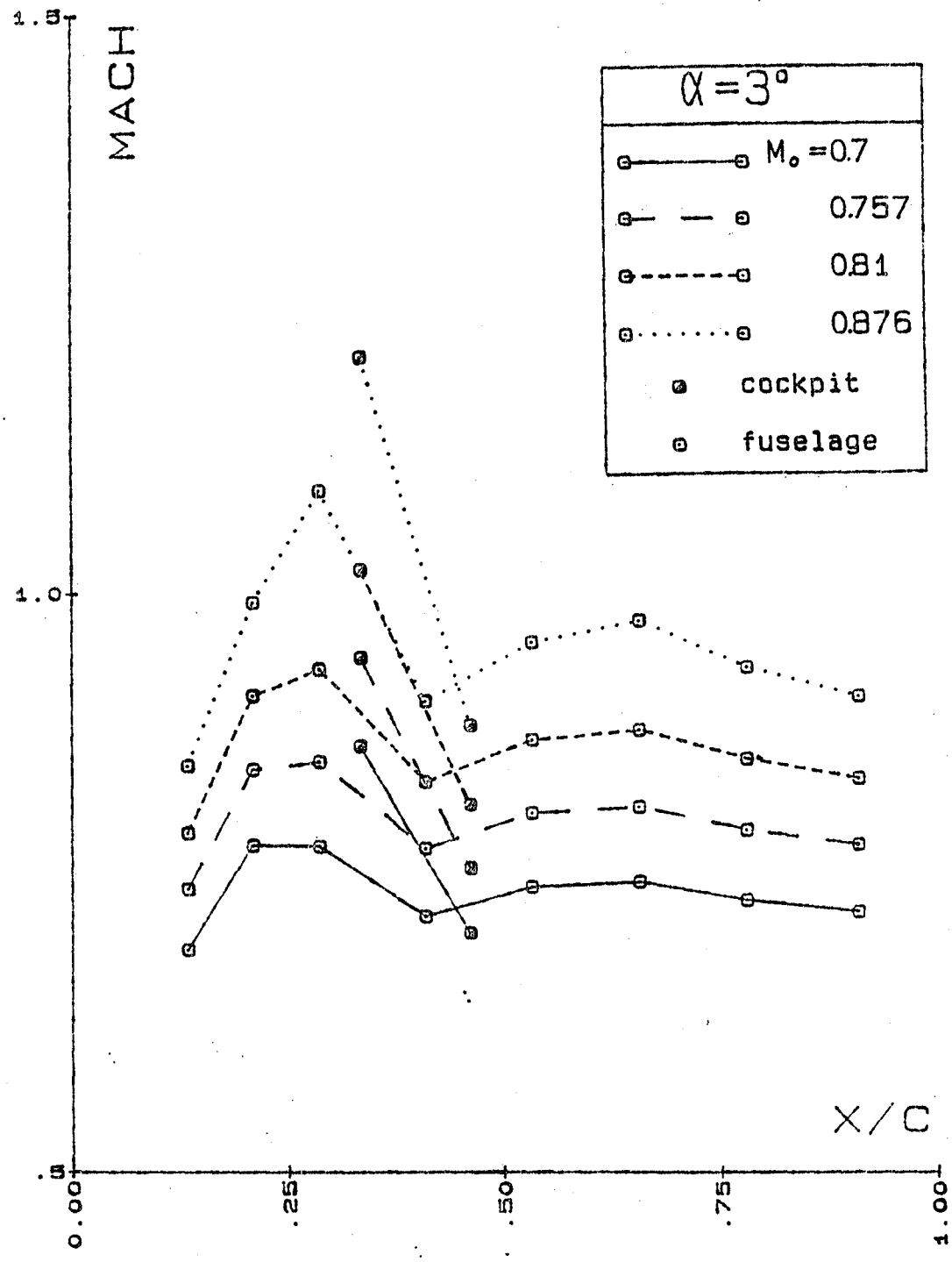

FIG 31: MACH NUMBER DISTRIBUTION ON THE CANARD MODEL (M_0 EFFEC

FLEXIBLE WALLS WITH CANARD MODEL

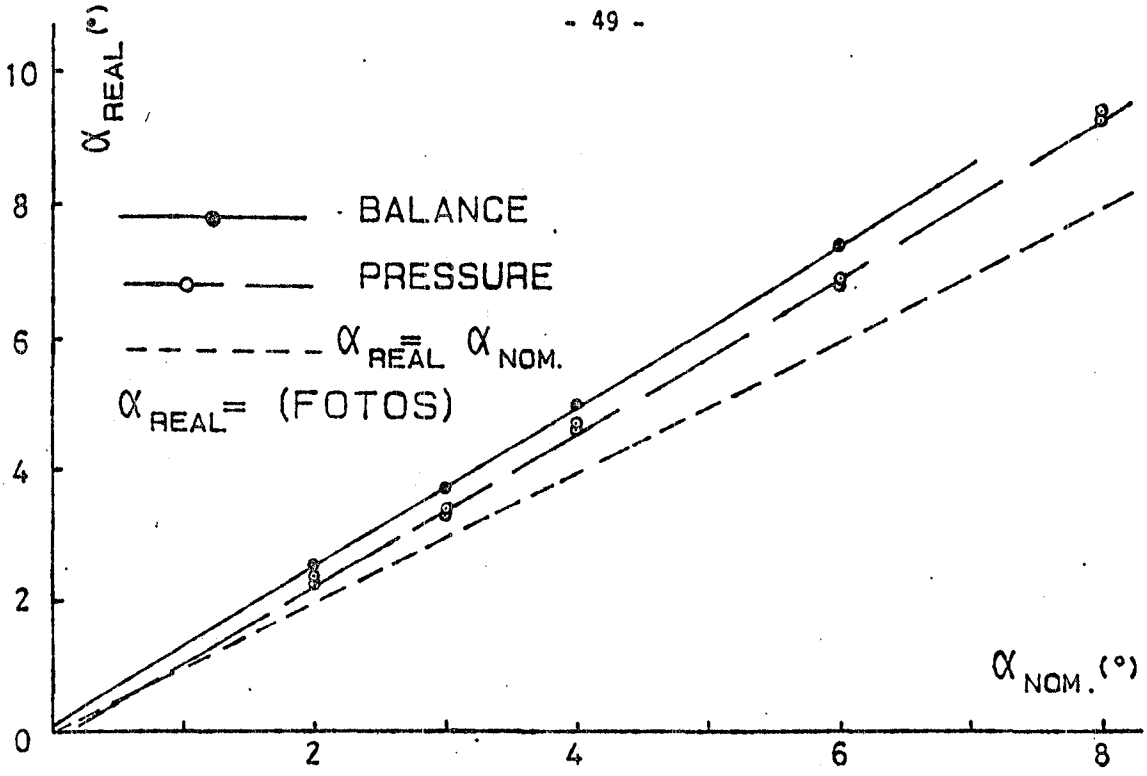

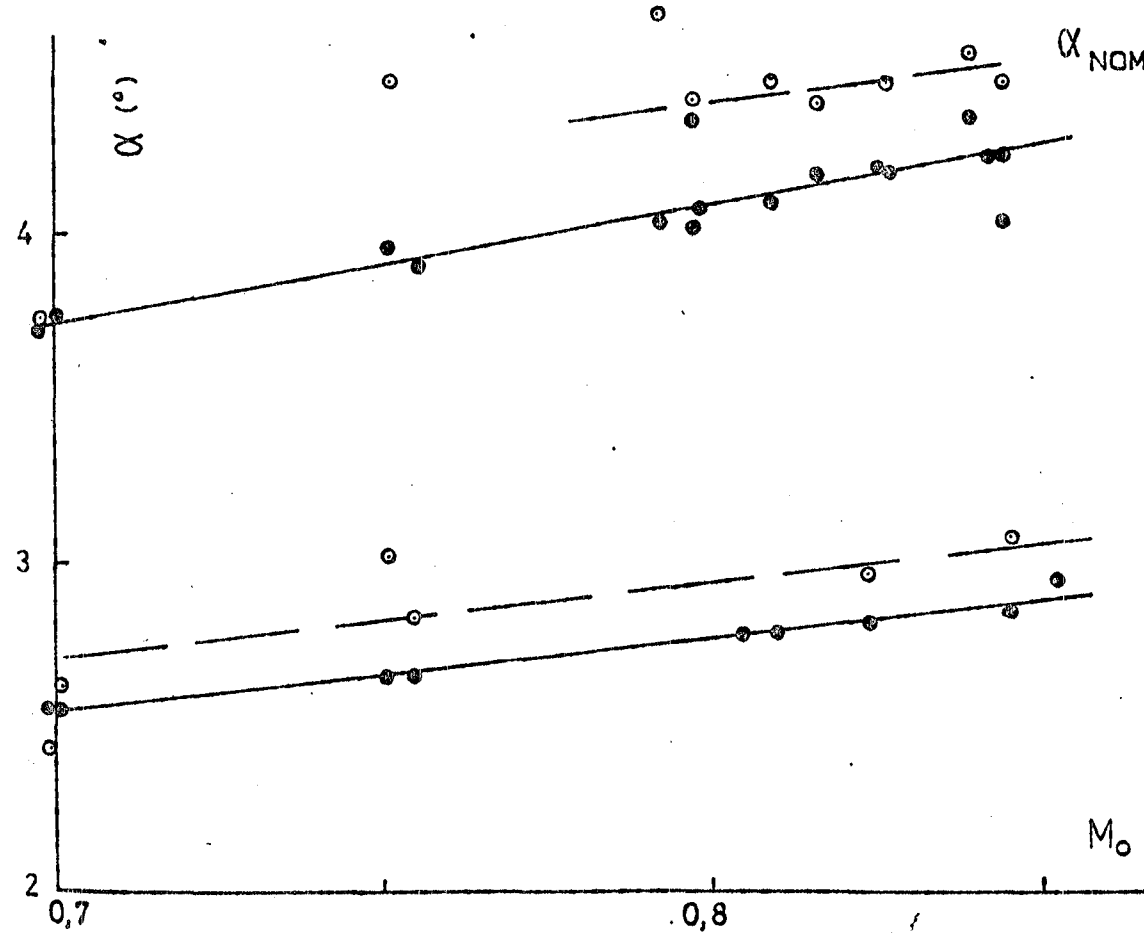

FIG 32: NOMINAL AND REAL (BALANCE OR FOTO) ANGLE OF ATTACK CANARD MODEL

End of Document